Halogen cycling and aerosol pH in the Hawaiian marine boundary layer

A. A. P. Pszenny, J. Moldanová, W. C. Keene, R. Sander, J. R. Maben, M. Martinez, P. J. Crutzen, D. Perner, R. G. Prinn

Atmos. Chem. Phys., 4, 147–168, 2004
www.atmos-chem-phys.org/acp/4/147/
SRef-ID: 1680-7324/acp/2004-4-147

Atmospheric Chemistry and Physics

Halogen cycling and aerosol pH in the Hawaiian marine boundary layer

A. A. P. Pszenny[1,*], J. Moldanová[2,3], W. C. Keene[4], R. Sander[2], J. R. Maben[4], M. Martinez[5], P. J. Crutzen[2,6], D. Perner[2], and R. G. Prinn[1]

[1]Center for Global Change Science, Massachusetts Institute of Technology, Cambridge, MA, USA
[2]Air Chemistry Division, Max Planck Institute for Chemistry, Mainz, Germany
[3]Swedish Environmental Research Institute, Göteborg, Sweden
[4]Department of Environmental Sciences, University of Virginia, Charlottesville, VA, USA
[5]Department of Meteorology, Pennsylvania State University, University Park, PA, USA; now at 2 (above)
[6]Scripps Institution of Oceanography, University of California at San Diego, La Jolla, CA, USA
[*]Now at: Institute for the Study of Earth, Oceans and Space, University of New Hampshire, Durham, and Mount Washington Observatory, North Conway, NH, USA

Received: 23 July 2003 – Published in Atmos. Chem. Phys. Discuss.: 5 September 2003
Revised: 16 January 2004 – Accepted: 21 January 2004 – Published: 3 February 2004

Abstract. Halogen species (HCl* (primarily HCl), Cl* (including Cl_2 and HOCl), BrO, total gaseous inorganic Br and size-resolved particulate Cl^- and Br^-) and related chemical and physical parameters were measured in surface air at Oahu, Hawaii during September 1999. Aerosol pH as a function of particle size was inferred from phase partitioning and thermodynamic properties of HCl. Mixing ratios of halogen compounds and aerosol pHs were simulated with a new version of the photochemical box model MOCCA that considers multiple aerosol size bins.

Inferred aerosol pHs ranged from 4.5 to 5.4 (median 5.1, n=22) for super-μm (primarily sea-salt) size fractions and 2.6 to 5.3 (median 4.6) for sub-μm (primarily sulphate) fractions. Inferred daytime pHs tended to be slightly lower than those at night, although daytime median values did not differ statistically from nighttime medians. Simulated pHs for most sea-salt size bins were within the range of inferred values. However, simulated pHs for the largest size fraction in the model were somewhat higher (oscillating around 5.9) due to the rapid turnover rates and relatively larger infusions of sea-salt alkalinity associated with fresh aerosols.

Measured mixing ratios of HCl* ranged from <30 to $250\,\mathrm{pmol\,mol^{-1}}$ and those for Cl* from <6 to $38\,\mathrm{pmol\,mol^{-1}}$. Simulated HCl and Cl* ($Cl + ClO + HOCl + Cl_2$) mixing ratios ranged between 20 and 70 pmol $\mathrm{mol^{-1}}$ and 0.5 and $6\,\mathrm{pmol\,mol^{-1}}$, respectively. Afternoon HCl* maxima occurred on some days but consistent diel cycles for HCl* and Cl* were not observed. Simulated HCl did vary diurnally, peaking before dusk and reaching a minimum at dawn. While individual components of Cl* varied diurnally in the simulations, their sum did not, consistent with the lack of a diel cycle in observed Cl*.

Mixing ratios of total gaseous inorganic Br varied from <1.5 to $9\,\mathrm{pmol\,mol^{-1}}$ and particulate Br^- deficits varied from 1 to $6\,\mathrm{pmol\,mol^{-1}}$ with values for both tending to be greater during daytime. Simulated Br_t and Br^- mixing ratios and enrichment factors (EFBr) were similar to those observed, with early morning maxima and dusk minima. However, the diel cycles differed in detail among the various simulations. In low-salt simulations, halogen cycling was less intense, Br^- accumulated and Br_t and EFBr increased slowly overnight. In higher-salt simulations with more intense halogen cycling, Br^- and EFBr decreased and Br_t increased rapidly after dusk. Cloud processing, which is not considered in this version of MOCCA, may also affect these diel cycles (von Glasow et al., 2003). Measured BrO was never above detection limit ($\approx 2\,\mathrm{pmol\,mol^{-1}}$) during the experiment, however relative changes in the BrO signal during the 3-hour period ending at 11:00 local time were mostly negative, averaging $-0.3\,\mathrm{pmol\,mol^{-1}}$. Both of these results are consistent with MOCCA simulations of BrO mixing ratios.

Increasing the sea-salt mixing ratio in MOCCA by ≈25% (within observed range) led to a decrease in O_3 of ≈16%. The chemistry leading to this decrease is complex and is tied to NO_x removal by heterogeneous reactions of $BrNO_3$ and $ClNO_3$. The sink of O_3 due to the catalytic Cl-ClO and Br-BrO cycles was estimated at -1.0 to $-1.5\,\mathrm{nmol\,mol^{-1}}$ $\mathrm{day^{-1}}$, a range similar to that due to O_3 photolysis in the MOCCA simulations.

Correspondence to: A. A. P. Pszenny
(alex.pszenny@unh.edu)

1 Introduction

Chemical reactions involving halogen radicals significantly influence the composition of the Earth's atmosphere. These reactions were first discussed in connection with stratospheric ozone loss, especially within the polar vortices during spring (e.g. Wennberg et al., 1994). The photochemical activation of tropospheric Cl and Br during polar sunrise episodically enhances oxidation of hydrocarbons (e.g. Jobson et al., 1994) and destruction of O_3 (Martinez et al., 1999 and references therein) in near-surface marine air. High concentrations of BrO and associated O_3 destruction have also been observed over salt flats near the Dead Sea and elsewhere (Hebestreit et al., 1999). In contrast, reactions of Cl atoms with hydrocarbons can enhance O_3 production in polluted urban air (Tanaka et al., 2000). Photolysis of I-containing organic compounds emitted by macroalgae in coastal regions initiates I-radical chemistry that may substantially increase production of new particles (O'Dowd et al., 2002).

Although significant and detectable with current technologies, the above influences of halogen radicals in the troposphere are limited in duration and/or spatial extent. However, the marine boundary layer (MBL) covers two thirds of the Earth's surface and contains the highest concentrations of sea-salt and many gaseous halogens in the atmosphere (e.g. Cicerone, 1981; Graedel and Keene, 1995). Although the global impact of halogen radical chemistry in terms of O_3 destruction (Dickerson et al., 1999; Galbally et al., 2000), S(IV) oxidation (Vogt et al., 1996; Keene et al., 1998), and related effects in the open-ocean MBL may be greater, they are considerably more difficult to identify there because of less intensive radical chemistry.

Most Cl and Br in the MBL originates from sea-salt aerosols produced by wind stress at the ocean surface (e.g. Gong et al., 1997). Fresh sea-salt aerosols rapidly dehydrate towards equilibrium with ambient water vapor and undergo other processes involving the scavenging of reactive gases, aqueous-phase transformations and volatilisation of products. Many of these other processes are strongly pH-dependent (Keene et al., 1998). In most MBL regions, sea-salt alkalinity is rapidly titrated (seconds to minutes) by ambient acids (Chameides and Stelson, 1992; Erickson et al., 1999) and, under a given set of conditions, the pHs of the super-μm, sea-salt size fractions approach similar values that are determined by HCl phase partitioning (Keene and Savoie, 1998, 1999; Keene et al., 2002). Most measurements of particulate Br in marine air reveal substantial depletions relative to conservative sea-salt tracers (e.g. Sander et al., 2003). Because HBr is highly soluble in acidic solution, these depletions cannot be explained by acid-displacement reactions (e.g. Ayers et al., 1999). The observed depletions are generally consistent with the predicted volatilisation of Br_2 and BrCl based on autocatalytic halogen activation mechanisms (Vogt et al., 1996):

$$HOBr + Br^- + H^+ \rightarrow Br_2 + H_2O \quad \text{(R1)}$$

$$HOCl + Br^- + H^+ \rightarrow BrCl + H_2O. \quad \text{(R2)}$$

Br_2 and BrCl then photolyse in sunlight to produce atomic Br and Cl. Most Br atoms recycle in the gas phase via the reaction sequence:

$$Br + O_3 \rightarrow BrO + O_2 \quad \text{(R3)}$$

$$BrO + HO_2 \rightarrow HOBr + O_2 \quad \text{(R4)}$$

$$HOBr + h\nu \rightarrow OH + Br \quad \text{(R5)}$$

and thereby catalytically destroy O_3, analogous to Br cycling in the stratosphere (e.g. Mozurkewich, 1995; Sander and Crutzen, 1996). In contrast, most atomic Cl in the MBL reacts with hydrocarbons via hydrogen extraction to form HCl vapor, which is relatively stable against chemical degradation. Consequently, HCl must recycle via a multiphase pathway to sustain significant Cl-radical chemistry without completely dechlorinating sea-salt aerosol (Keene et al., 1990; Graedel and Keene, 1995).

Observational evidence in support of the above scenario in the background MBL is limited in extent and in some cases controversial. Direct measurements of BrO by differential optical absorption spectroscopy (DOAS) in coastal air (Hönninger, 1999) and over the open ocean (Leser et al., 2003) indicate mixing ratios that are near or below analytical detection limits of about 1 to 3 pmol mol^{-1} but within the range of model predictions. Although column-integrated DOAS observations from space reveal higher mixing ratios of tropospheric BrO (e.g. Wagner and Platt, 1998), the relative amounts in the MBL cannot be resolved. Strong diel anticorrelations between total volatile inorganic Br and particulate Br have been reported (e.g. Rancher and Kritz, 1980) but the lack of speciation precludes unambiguous interpretation.

Other measurements suggest that, under some conditions, Cl-atom precursors are produced and accumulate to significant mixing ratios (greater than 100 pmol mol^{-1} Cl) in the dark (Pszenny et al., 1993; Spicer et al., 1998). Photolysis of these precursors following sunrise would sustain significant concentrations of atomic Cl ($>10^4$ cm^{-3}) during the early morning. Chlorine atom concentrations of this order have been inferred from relative concentration changes in hydrocarbons measured during some field campaigns (Singh et al., 1996a; Wingenter et al., 1996). However, model calculations based on the autocatalytic mechanism predict only minor accumulation of Cl-atom precursors at night and low concentrations of atomic Cl during the day (Keene et al., 1998) relative to those inferred from these measurements (Pszenny et al., 1993; Singh et al., 1996b; Wingenter et al, 1996; Spicer et al., 1998). In addition, other studies based on observed relative concentration changes in hydrocarbons (Parrish et al., 1993; Jobson et al., 1998) and the global C_2Cl_4 budget (Singh et al., 1996b) suggest minor to insignificant influences of Cl-radical chemistry in the MBL. It is thus evident that the

nature of chemical transformations involving inorganic halogens in the MBL and their overall impacts on the composition of the global troposphere are very uncertain.

To help reduce these uncertainties, a multiphase suite of inorganic Cl and Br species and related chemical and physical conditions was measured in the relatively clean easterly trade-wind regime over the North Pacific Ocean at Hawaii during September 1999. In this paper, these data are evaluated for consistency with expectations based on the halogen activation mechanism and associated implications for oxidation processes in the remote MBL are assessed.

Although evidence is now mounting that the cycling of reactive iodine compounds may also significantly influence the chemical evolution of MBL air (e.g., McFiggans et al. 2000, and references therein), measurements of aerosol I species were beyond the scope of this effort. Due to this lack of multiphase observational constraints on I cycling the discussion is limited to Cl and Br chemistry.

2 Methods

2.1 Site description

Between 4 and 29 September 1999 (Julian days 248–273), size-resolved marine aerosols and reactive trace gases were sampled at Bellows Air Force Station on the windward coast of Oahu, Hawaii (21°22.0′ N, 157°42.8′ W). Unless otherwise noted, air was sampled from the top of a 20-m scaffolding tower on the beachfront and samples were processed in adjacent laboratory containers. Marine air associated with the persistent easterly trades flowed over the site almost continuously for the duration of the experiment. Aerosol sampling was suspended during precipitation events and on rare occasions when winds were along- or offshore. During low tides, waves breaking over shallow reefs approximately 2 km upwind may have influenced the composition of sampled air relative to that farther offshore. However, no discernable correlations were detected between the measurements and local tidal cycles suggesting that such influences were negligible.

2.2 Chemical measurements

Ambient aerosols were sampled during six, one- to three-day intensives covering a total of eleven diel cycles. Twenty-two discrete daytime and nighttime samples (nominal 12-hour duration) were collected using a modified (with the addition of a top "0" stage) Graseby-Anderson 235 cascade impactor configured with a Liu-Pui type inlet, polycarbonate substrates, and quartz-fiber backup filters (Pallflex 2500 QAT-UP) (e.g. Pszenny et al., 1989; Zhu et al., 1992; Keene et al., 2002). At an average sampling rate of $1.13\,m^3\,min^{-1}$, approximate ambient geometric mean diameters (GMDs) for the sampled size fractions were 21, 11, 5.2, 2.4, 1.3, 0.65, and 0.33 μm. The GMD of the largest fraction was calculated as $\sqrt{2}$ times the theoretical 50% cut diameter of the stage "0" jet plate. The GMD of the smallest fraction was calculated as the theoretical 50% cut diameter of the next largest stage divided by $\sqrt{2}$. Bulk aerosol was sampled in parallel on quartz-fiber filters at an average flow rate of $1.3\,m^3\,min^{-1}$. All air volumes reported were normalised to standard temperature and pressure (0°C, 1 atm). Impactors and bulk-filter cassettes were cleaned, dried, loaded, and unloaded in a Class 100 clean bench. Exposed substrates and filters were transferred to polypropylene tubes, stored in glass jars to minimise gas exchange, frozen, and transported to the University of Virginia (UVA) for chemical analysis. Dynamic field blanks were mounted, exposed by drawing ambient air for one minute, and subsequently processed and analysed using the same procedures as those for samples.

At UVA, half sections of substrates were extracted under sonication in 10 mL of $>18\,M\Omega\,cm^{-1}$ deionized water (DIW) and entire exposed backup and bulk filters were extracted in 40 mL DIW. Extracts were analysed for Mg^{2+}, Ca^{2+}, Na^+ and K^+ by atomic absorption spectrophotometry, NH_4^+ by automated colorimetry, and NO_3^-, Cl^-, Br^-, SO_4^{2-}, $CH_3SO_3^-$, and $C_2O_4^{2-}$ by high-performance ion chromatography (IC) (Keene and Savoie, 1998; Keene et al., 2002). Data for samples were corrected based on averages for the field blanks. Overall measurement precisions and detection limits (DLs) for particulate species (and for volatile Cl and total gaseous inorganic Br, see below) were estimated following Keene et al. (1989). Precision for Br^-, $CH_3SO_3^-$, and $C_2O_4^{2-}$ averaged ±15% to ±20%; precision for other analytes averaged about ±10%. Sea-salt and non-sea-salt (nss) constituents were differentiated using Mg^{2+} as the reference species (Keene et al., 1986). Mg^{2+} rather than Na^+ was employed because its background in the quartz-fiber sampling media was relatively lower (compared to sea-salt ratios) and less variable than that for Na^+ and thereby provided more precise results for filter samples (the $<0.65\,\mu$m GMD size fraction and bulk aerosol).

Internal losses of super-μm aerosols within Sierra-type cascade impactors average about 25% to 30%; other sources of bias for size-resolved particulate analytes based on these procedures are generally unimportant (Keene et al., 1990; and references therein). Conjugate anions and cations of gases with pH-dependent solubility such as HCl and NH_3 are generally not conservative when populations of chemically distinct aerosols (e.g. super-μm sea salt and sub-μm S) are sampled in bulk (e.g. Keene et al., 1990). Consequently, measurements of these species in bulk samples are potentially unreliable and not considered herein. However, concentrations of most particulate analytes (including Br^- and nss SO_4^{2-}) are conservative in bulk samples. Relative to the corresponding sums over all size fractions, concentrations in bulk samples are both more precise and not subject to bias from internal losses within impactors. Consequently, data for conservative species in bulk samples offer greater resolution for some assessments reported below.

Volatile inorganic Cl gases were measured in parallel using the tandem mist chamber technique (Keene et al., 1993; Maben et al., 1995; Keene and Savoie, 1998). Air was sampled over 121 discrete 2-hour intervals at a nominal rate of 16 L min^{-1} through a size-segregating inlet that inertially removed super-μm-diameter aerosol from the air stream followed by an in-line Teflon filter (Zefluor 2-μm pore diameter) that removed sub-μm-diameter aerosol. Mist chamber samplers were positioned in tandem downstream of the inlet. The upstream chamber contained acidic solution (37.5 mM H_2SO_4 and 0.042 mM $(NH_4)_2SO_4$) to sample HCl^* (primarily HCl); the downstream chamber contained alkaline solution (30.0 mM $NaHCO_3$ and 0.408 mM $NaHSO_3$) to sample Cl^* (including Cl_2 and HOCl). Total inorganic Cl (Cl_t) was sampled in parallel using a similar system configured with tandem mist chambers, both of which contained alkaline solutions. Cl_t is approximately equal to HCl^*+Cl^* and thereby provides an independent quality constraint on the data. Sample air volumes were measured with mass flow meters; the meters were plumbed in series and compared with a factory-calibrated meter traceable to the National Institute of Standards and Technology (NIST) immediately before and after the field intensive. Field blanks were generated at the beginning and end of each diel intensive by loading and drawing ambient air through mist solutions for 15 seconds. Blanks were subsequently processed using the same procedures as those for samples. Chloride in mist solutions was quantified on site (usually within a few hours after sampling) by IC using matrix-matched standard solutions traceable to NIST. Collection efficiencies and specificities for the Cl gases were reported by Maben et al. (1995). HCl^* was precise to $\pm$20% or $\pm$15 pmol mol^{-1}, whichever was the greater absolute value. Prior to 20 September, Cl^* and Cl_t were precise to $\pm$20% or $\pm$10 pmol mol^{-1}, whichever was greater. Thereafter, modification of the analytical technique improved precision to $\pm$3 pmol mol^{-1} and Cl_t to $\pm$15% or $\pm$5 pmol mol^{-1}, whichever was greater.

Volatile inorganic Br (Br_t) was sampled at a nominal rate of 85 L min^{-1} in parallel with size-segregated and bulk aerosols using a filter pack technique (Rancher and Kritz, 1980; Li et al., 1994). An open-face, three-stage, 47-mm, polycarbonate filter pack housing was loaded with a quartz-fiber (Pallflex 2500 QAT-UP) particle filter followed by tandem rayon filters (Schleicher and Schuell, Grade 8S) impregnated with a solution of 10% K_2CO_3 and 10% glycerol (e.g. Bardwell et al., 1990). Collection efficiencies by the upstream impregnated filter were indistinguishable from 100% (i.e. no detectable breakthrough). Sampling rates were measured with a mass flow meter. Filter packs were cleaned, dried, loaded, and unloaded in a class 100 clean bench. Exposed filters were transferred to polypropylene tubes, stored in glass jars, frozen, and transported to UVA for chemical analysis. Field blanks were generated using procedures similar to those for aerosols. Samples were extracted under sonication in 5 mL DIW and analysed for Br^- by IC using matrix-matched standard solutions. The average precision was $\pm$17% or $\pm$0.7 pmol mol^{-1}, whichever was the greater absolute value.

BrO, NO_2 and O_3 were measured continuously with a long-path DOAS (Platt and Perner, 1983; Platt, 1994; Martinez et al., 1999, 2000). DOAS quantifies trace gases based on distinct narrow absorption features in the UV-VIS spectral region. Light from a white light source (Hanovia L5269, Xe arc) is directed along an open path of several kilometers through the atmosphere by a parabolic mirror (diameter of 0.3 m, focal length of 0.28 m), reflected by an array of 30 retroreflectors of 5-cm diameter each and collected back at the source by a second mirror (diameter of 0.5 m, focal length of 1.25 m) which focuses the light into a 0.6-mm quartz fiber. The quartz fiber channels the light into a spectrograph. Column densities of trace gases are obtained from the differential optical densities of distinct absorption features and yield integrated concentrations along the light path. For this experiment the receiving mirror was mounted on the roof of a laboratory container at the base of the tower and the retroreflector array was positioned on the roof of a building on a pier approximately 6.5 km to the southeast. This configuration allowed an unobstructed path at an average height of approximately 7 m over near-shore coastal ocean.

The spectrograph, designed and built at the Max-Planck-Institut für Chemie, is based on a holographic grating (American Holographic 455.01, flat field region 240–800 nm, 550 grooves/mm, focal length 212 mm, dispersion about 7 nm/mm). Recorded spectra covered the wavelength range between 290 and 460 nm, with a spectral resolution of 0.9 nm. The RY-1024 detector from Scientific Instruments, GmbH (Hamamatsu photodiode array cooled to $-70°$C) is mounted on translation tables for selection of the spectral region and in order to correct for the pixel-to-pixel diode variation of the array by the Multi-Channel Scanning Technique (MCST) (Brauers et al., 1995). A complete spectrum was recorded approximately every 10 min.

The trace gas column densities along the light path were derived from their proper absorbances, which are determined from a simultaneous least-squares fit of reference spectra of all trace compounds and of a polynomial to the air spectrum (Stutz and Platt, 1995). The reference spectrum for NO_2 was obtained from a quartz cell filled with the gas placed in the light path. Ozone and halogen oxide spectra recorded in the laboratory prior to deployment to the field were wavelength calibrated according to the NO_2 spectrum. Ozone was produced in the lab by flowing oxygen through a silent discharge, and BrO was generated by irradiating mixtures of Br_2 and O_3 with 254-nm mercury light (Philips TUV 40 W).

The differential absorption cross sections required for the calculation of concentrations were obtained by folding the higher-resolution cross sections (Bass et al., 1984; Wahner et al., 1988; Laszlo et al., 1995; Harder et al., 1997) with Hg-line spectra as resolved by the instrument (Platt, 1994). The temperature dependencies of the spectra of O_3 and BrO were

taken into account. The actual value for the BrO differential absorption cross section at 338 nm was 6.2×10^{-18} cm^2 at 298 K. Application of the MCST diminished the latter value to 6.1×10^{-18} cm^2.

The systematic errors derived for the concentrations are caused mainly by lamp structures (the main limitation of detection) and by uncertainties of the absorption coefficients (3–20%). Statistical errors arise from photon statistics, from detector noise and from random residual instrument structures. Average absolute detection limit for BrO was about 2 pmol mol^{-1} and that for O_3 was about 10 nmol mol^{-1}, depending on visibility.

In a second evaluation of the BrO detection limit, an air spectrum measured a few hours earlier was fitted to the actual air spectrum together with the reference spectra to minimise systematic errors caused by lamp structures, which change over time. Only changes in mixing ratios can be obtained this way, but the detection limits for changes in BrO, determined by the 2-sigma uncertainty of the fit, are about a factor of two lower than for absolute BrO mixing ratios, with a median of 1 pmol mol^{-1}.

IO, OClO and HCHO were also measured but never exceeded their respective detection limits of approximately 1.5, 1.5 and 400 pmol mol^{-1}. NO_2 exceeded its detection limit of approximately 60 pmol mol^{-1} only during brief periods of offshore flow. NO_3 data were not acquired because this molecule absorbs in a different spectral region that was not monitored.

2.3 Meteorological measurements and ancillary data

Wind direction, wind speed, air temperature, and relative humidity (RH) were measured continuously at the top of the tower with instruments maintained by the University of Hawaii. Ten-minute averages were provided for the first two intensive sampling periods and one-minute averages thereafter (S. Howell, personal communication, 1999). "Clean sector" winds were defined as coming from azimuths between 35° and 120° at speeds greater than 1 m s^{-1}.

Five-day, three-dimensional back trajectories were calculated at MIT using version 4.0 of the NOAA/ARL HY-SPLIT model (Draxler, 1995) and three-dimensional wind fields from the EDAS (early ETA model Data Analysis System), which includes both analyses and forecasts. Trajectories ending at five altitudes (0.3, 1.5, 2.5, 5 and 9 km) above the sampling site at 00:00, 06:00, 12:00 and 18:00 UT (Universal Time) were calculated for each day of an intensive.

2.4 Thermodynamic calculations

Equilibrium hydrogen ion activities for individual aerosol size fractions were calculated based on the measured phase partitioning and associated thermodynamic properties of HCl following the approach of Keene and Savoie (1998). Briefly, the equilibrium

$$HCl_g \overset{K_H}{\rightleftharpoons} \{HCl_{aq}\} \overset{K_{a\mathrm{HCl}}}{\rightleftharpoons} \{H^+\} + \{Cl^-\} \quad (1)$$

was evaluated based on simultaneous measurements of HCl_g (assumed equal to HCl*) and particulate Cl^- concentrations in air, the Henry's Law (K_H) and acid dissociation constants ($K_{a\mathrm{HCl}}$) and associated temperature corrections for HCl (Marsh and McElroy, 1985), liquid water contents (LWCs) for sea-salt dominated size fractions calculated from hygroscopicity models (e.g. Gerber, 1985; Gong et al., 1997), and activity coefficients (Pitzer, 1991). LWCs for the three smallest size fractions were modeled following Keene et al. (2002) based on Tang and Munkelwitz (1994). HCl_g mixing ratios, RHs, and temperatures used in the calculations were averaged over the corresponding aerosol sampling intervals. Total acidities (H_{tot}=H^++undissociated acids) for individual aerosol size fractions were estimated based on evaluation of the sulphate-bisulphate equilibrium (Keene et al., 2002):

$$\{H^+\}\times\{SO_4^{2-}\}=\{HSO_4^-\}\times K_{a\mathrm{HSO_4^-}}. \quad (2)$$

2.5 Photochemical model calculations

Multiphase chemical processes were simulated using the box Model Of Chemistry Considering Aerosols (MOCCA) (e.g. Sander and Crutzen, 1996; Vogt et al., 1996, Sander et al., 1999). The chemical mechanism considers reactions both in the gas phase and in deliquesced sea-salt and nss sulphate aerosols. Photochemical reaction rates, assuming clear-sky conditions, vary as a function of solar zenith angle. The reaction mechanism includes Cl, Br, I and S compounds and reactions in addition to the standard tropospheric HO_x, CH_4 and NO_x chemistry. Further information about the model is available at http://www.mpch-mainz.mpg.de/~sander/mocca/.

A new version of the model that evaluates chemical processes involving multiple aerosol size fractions was developed for this analysis. The model was initialised with externally mixed populations of unreacted sea-salt aerosols and pre-existing sulphate aerosols. Sea-salt size bins were centered on diameters of 21, 11, 5.2, 2.4, 1.3, 0.65 and 0.33 μm. The initial concentrations of nss SO_4^{2-} were partitioned into seven size bins with diameters of 2.4, 1.3, 0.65, 0.33, 0.17, 0.09, and 0.05 μm (i.e. the smallest measured size fraction was represented by four model bins with diameters of 0.33, 0.17, 0.09 and 0.05 μm). The total particle volume in each size bin was calculated from the equilibrium molality of sea-salt (Tang, 1997) and NH_4HSO_4 (Tang and Munkelwitz, 1994) solutions at the measured ambient relative humidity. The densities of the equilibrium solutions were calculated using parameters of Clegg and Whitfeldt (1991) for sea-salt and of Tang and Munkelwitz (1994) for NH_4HSO_4. The Kelvin effect was considered for the sub-μm size fractions. The average atmospheric lifetimes of particles in each

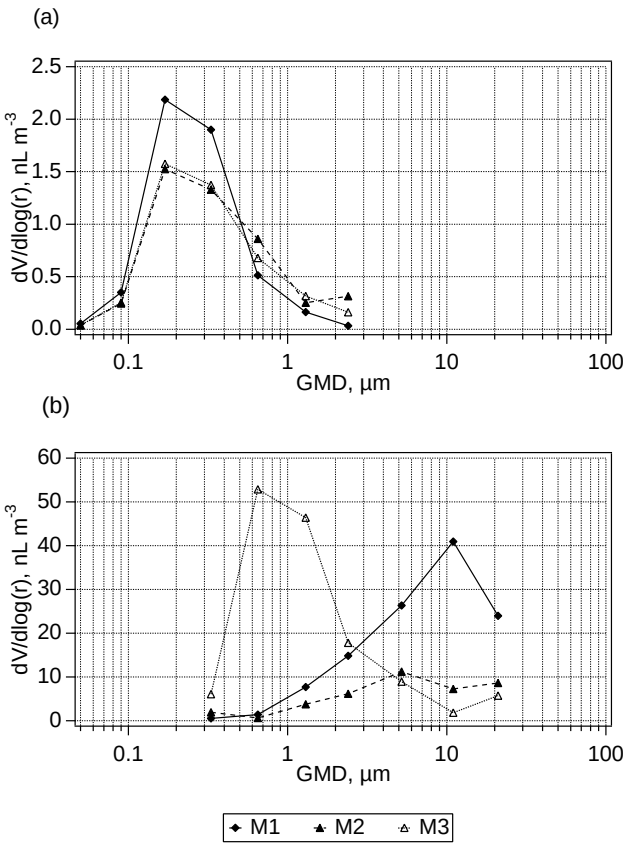

Fig. 1. Volume size distributions of sulphate **(a)** and sea-salt **(b)** aerosols used in model simulations. Distributions for simulation M4 were identical to those for simulation M1.

size bin against dry deposition to the sea surface were based on Slinn and Slinn (1980). Emissions of sea-salt particles were equated to their dry-deposition fluxes thereby maintaining constant atmospheric concentrations. At each time step, fresh aerosol was added to, and an equivalent amount of reacted aerosol removed from, each sea-salt size bin in proportion to the corresponding atmospheric lifetime. This procedure sustained finite thermodynamic disequilibria for the internally mixed aerosols in each sea-salt size fraction; the magnitude of disequilibrium increased with particle size. During simulations, nss SO_4^{2-} accumulated in both sea-salt and sulphate aerosols via dissolution and oxidation of SO_2 and condensation of H_2SO_4.

Initial conditions for model runs are summarised in Table 1 and Fig. 1. Processes were simulated over a range of conditions to investigate multiphase variability in bromine species, differences in chlorine and bromine volatilisation as a function of particle size, and the sensitivity of O_3 to halogen chemistry.

3 Results and discussion

3.1 Meteorological condition summaries for intensive sampling periods

The meteorological data obtained on the tower and NO_3^- and nss SO_4^{2-} concentrations measured in cascade impactor samples collected during each intensive are summarised in Table 2. The back-trajectories indicated that large-scale anticyclonic flow of variable strength delivered air to the vicinity of the Hawaiian Islands throughout the experiment. No recent (i.e. within the five days represented by the trajectories) continental influence was suggested by any of the trajectories calculated for the first five intensive periods. During Intensive #6, however, the trajectories at all except the 9 km endpoint level indicated relatively vigorous anticyclonic flow. A distinctive feature in this trajectory set was the 5 km endpoint trajectories from the beginning of the period through 27 September, 00:00 UT, which suggested that air at this end-point altitude had passed close to and perhaps over the northwest U.S. – southwest Canadian shoreline at high altitude three to four days before arriving at the site. These 5 km endpoint trajectories suggested further that prior to about 4 days back, the air at this endpoint level may have been transported rapidly across the mid-latitude North Pacific from Asia. The 27 September, 06:00 UT 5 km endpoint trajectories and subsequent ones indicated much less rapid, more localised flow. Nitrate and nss SO_4^{2-} concentrations peaked later in the period (sample collected 27 September, 16:31 UT to 28 September, 04:10 UT). The back trajectories in combination with the relatively high NO_3^- and nss SO_4^{2-} concentrations observed during this period strongly suggest that continental pollutants were transported into the vicinity of Hawaii early during (and perhaps prior to) the period and then affected the air sampled near-surface after roughly a one-day delay.

3.2 Aerosol acidity

We inferred aerosol pH by evaluating the thermodynamic equilibrium between gas-phase HCl and aqueous Cl^-. Results are summarised in Table 3. Several potential sources of error are associated with this method. These include uncertainties in field measurements (HCl, particulate Cl^-, RH and temperature), reliability of the hygroscopic growth models and associated assumptions involved in estimating aerosol LWCs, accuracy of Henry's Law and acid dissociation constants for HCl, and the assumption that the multiphase system is at thermodynamic equilibrium with respect to HCl. Measurement uncertainties are described above and, in most cases, correspond to relatively minor sources of error in inferred acidity ($<\pm 0.1$ pH unit). LWCs estimated using different models (e.g. Gerber, 1985; Tang, 1997 for sea-salt) generally agree within about $\pm 25\%$ and, consequently, also

Table 1. (a) Description of aerosol and ozone mixing ratio in MOCCA model simulations.

Model simulation	Aerosol volume (nL m^{-3})		Volume mean diameter (μm) / number mean diameter (μm)		Ozone mixing ratio
	Sea-salt	Sulphate	Sea-salt	Sulphate	nmol mol^{-1}
M1	28.6	1.4	8.98/0.59	0.32/0.10	20
M2	10.1	1.2	7.45/0.37	0.48/0.10	20
M3	36.0	1.2	2.10/0.50	0.44/0.10	20
M4	28.6	1.4	8.98/0.59	0.32/0.10	30

Table 1. (b) Initial conditions common to all MOCCA simulations.

General conditions		
temperature	297.65	K
pressure	1013.25	hPa
relative humidity	71.8	%
latitude	21.35	degrees
height of MBL	1000	m
Initial mixing ratios in gas phase		
H_2O_2	600	pmol mol^{-1}
NH_3	100	pmol mol^{-1}
NO_2	20	pmol mol^{-1}
HNO_3	5	pmol mol^{-1}
CH_4	1.8	μmol mol^{-1}
HCHO	300	pmol mol^{-1}
CO	70	nmol mol^{-1}
CO_2	350	μmol mol^{-1}
HCl	40	pmol mol^{-1}
DMS	60	pmol mol^{-1}
SO_2	90	pmol mol^{-1}
Alkenes	100	pmol mol^{-1}
Alkanes	500	pmol mol^{-1}
Concentrations in RH-equilibrated sea-salt particles*		
$[Cl^-]$	5.75	M
$[Br^-]$	0.0089	M
$[HCO_3^-]$	0.022	M
$[SO_4^=]$	0.30	M
Concentrations in RH-equilibrated sulphate particles*		
$[HSO_4^-] + [SO_4^=]$	3.61	M
$[NH_4^+]$	1.81	M
Emissions rates e		
eNO	0.024	g m^{-2} $year^{-1}$
$e$$NH_3$	0.009	g m^{-2} $year^{-1}$
eDMS	0.082	g m^{-2} $year^{-1}$

* Without Kelvin effect

correspond to relatively minor uncertainties in calculated aerosol acidity ($<\pm 0.1$ pH unit, Keene and Savoie, 1998).

Uncertainty in the Henry's Law constant for HCl corresponds to a potentially large source of error for this approach (Keene and Savoie, 1999). Published constants for HCl vary over three orders of magnitude (see Sander, 1999). The value used for the calculations reported herein (1.1 M atm^{-1}, Marsh and McElroy, 1985) is similar to that reported by Brimblecombe and Clegg (1989) but is at the lower limit of published values. If the actual Henry's Law constant for HCl is greater, aerosol acidities must be proportionately greater to sustain the measured phase partitioning. In this regard, we note that the average acidities of the super-μm sea-salt size fractions inferred from measured HCl phase partitioning under moderately polluted conditions at Bermuda (pH 3.5 to 4.5, Keene and Savoie, 1999) were within the range of individual detectable values estimated from direct acidity measurements under comparable conditions at the same location the following year (pH 3.3 to 5.5 with only two greater than 5.0, Keene et al., 2002). The consistency of these results suggests that the Henry's Law constant adopted herein (and by Keene and Savoie, 1999) is probably close to the true value.

Finally, this approach is based on the evaluation of thermodynamic equilibrium. Although sub-μm aerosols equilibrate rapidly with the gas phase, non-equilibrium conditions for the larger aerosol size fractions (e.g. Meng and Seinfeld, 1996) could introduce bias in calculated acidities. However, kinetic models suggest that most sea-salt alkalinity in most remote marine regions is rapidly titrated and near-equilibrium pH is established within seconds to tens of minutes after aerosol formation (Chameides and Stelson, 1992; Erickson et al., 1999). Corresponding lifetimes for most sea-salt aerosols against dry deposition are many hours to a few days. Although the chemical composition of recently acidified sea-salt continues to evolve toward equilibrium with the gas phase via incorporation of acids and volatilisation of HCl, model calculations indicate that aerosol pH is regulated by HCl phase partitioning and, thus, under a given set of conditions, remains relatively constant after the initial alkalinity has been titrated (Keene and Savoie, 1998, 1999; Erickson et al., 1999). In addition, the super-μm aerosol

Table 2. Summary of meteorological and other ancillary data for each aerosol sample interval. Median values are given for meteorological data obtained on the tower. NO_3^- and nss SO_4^{2-} values given are the sums over all stages of the cascade impactor sample collected during each intensive.

Start (UT, 1999)	End (UT, 1999)	WDir (°True)	WSpd ($m\,sec^{-1}$)	T (°C)	RH (%)	% in sector	NO_3 ($nmol\,m^{-3}$)	nss SO_4^{2-} ($nmol\,m^{-3}$)
Intensive 1								
4 Sep, 04:50	4 Sep, 16:18	071	6.9	25.0	69.5	100.	4.3	4.7
4 Sep, 16:30	5 Sep, 05:00	070	6.6	25.3	67.2	100.	4.9	5.0
Intensive 2								
7 Sep, 04:55	7 Sep, 16:07	063	4.8	25.1	74.9	100.	2.0	2.3
7 Sep, 16:19	8 Sep, 04:16	051	6.1	25.6	68.6	100.	3.5	4.5
Intensive 3								
11 Sep, 04:30	11 Sep, 16:10	089	5.4	25.1	69.7	99.9	4.1	4.1
11 Sep, 16:30	12 Sep, 04:10	079	4.3	25.6	72.0	75.6	3.6	3.6
12 Sep, 04:30	12 Sep, 16:06	070	5.5	25.1	71.1	100.	3.3	3.9
12 Sep, 16:30	13 Sep, 04:00	064	5.9	25.6	68.7	100.	2.5	3.1
Intensive 4								
16 Sep, 04:30	16 Sep, 16:09	077	6.8	25.2	69.3	100.	3.2	4.1
16 Sep, 16:36	17 Sep, 04:15	077	5.9	25.6	72.2	83.6	2.6	4.2
17 Sep, 04:25	17 Sep, 16:15	071	6.1	25.2	72.3	100.	3.0	4.5
17 Sep, 16:33	18 Sep, 04:10	073	5.9	25.8	70.3	98.6	3.4	4.8
Intensive 5								
20 Sep, 16:30	21 Sep, 04:10	067	5.5	25.6	68.4	100.	1.5	2.6
21 Sep, 04:33	21 Sep, 16:10	067	5.4	24.8	71.3	97.0	1.2	2.0
21 Sep, 16:32	22 Sep, 04:15	073	6.5	25.5	70.0	100.	2.6	2.4
22 Sep, 04:39	22 Sep, 16:15	075	7.2	25.1	72.8	97.8	2.5	2.9
Intensive 6								
26 Sep, 04:30	26 Sep, 16:10	085	6.3	25.3	75.1	96.9	3.2	3.8
26 Sep, 16:30	27 Sep, 04:10	073	5.3	25.8	74.9	100.	5.4	4.4
27 Sep, 04:36	27 Sep, 16:10	073	5.0	25.1	75.3	100.	4.7	5.0
27 Sep, 16:31	28 Sep, 04:10	058	4.0	25.5	66.0	93.9.	9.0	6.5
28 Sep, 05:28	28 Sep, 16:10	082	2.2	24.3	80.8	48.1	4.1	5.5
28 Sep, 16:30	29 Sep, 04:10	072	4.6	25.7	73.2	100.	3.3	4.1

size fractions at Hawaii exhibited small Cl^- deficits relative to sea-salt (Table 3) and, consequently, the small (<20%) changes in aqueous Cl^- concentrations between fresh and fully equilibrated sea-salt would have only minor influences on calculated acidities (<0.1 pH unit). Based on the above, the pHs of acidified aerosols estimated using this approach are probably reliable to about ±0.2 to ±0.3 pH unit.

The inferred equilibrium pHs for all aerosol size fractions analysed during the experiment were acidic (Table 3). Calculated pHs for super-μm fractions ranged from 4.5 to 5.4 with a median value of 5.1. Acidities of 0.65-μm size fractions were relatively greater (median pH of 4.6) and more variable (Table 3). Most Cl^- concentrations in the $<0.65\,\mu$m size fraction were less than the detection limit thereby precluding the application of this approach to estimate corresponding acidities. The greatest aerosol acidities during the experiment were associated with the apparent pollution transport episode on 28 September 1999. Aerosol pHs during that period fell within the upper range of reported values for moderately polluted conditions over the western North Atlantic Ocean (Keene and Savoie, 1999; Keene et al., 2002).

Laskin et al. (2003) recently hypothesized based on laboratory experiments that the reaction $OH+Cl^- \rightarrow OH^-+Cl$ at the surfaces of deliquesced sea-salt aerosols slows aerosol acidification and, thus, speeds S(IV) oxidation by O_3 during daytime in clean marine air. Data generated during this experiment were examined for evidence in support of this hypothesis. Median pH values inferred from HCl phase partitioning for each of the six largest size fractions did not differ statistically day vs. night (Mann-Whitney U tests, α=0.05), although the median in each fraction was 0.1 to 0.2 pH unit lower during the day than at night (Fig. 2a). Nss-SO_4^{2-} distributions also differed insignificantly day vs. night (Fig. 2b). Both of these observations are in agreement with MOCCA simulation results (Fig. 3b). HCl* mixing ratios, with 2-hour time resolution, provide a diagnostic of aerosol acidity during midday. HCl is infinitely soluble in alkaline solution and its uptake is diffusion limited. Significant production of alkalinity during midday would favor HCl partitioning into the aerosol and, thus, smaller HCl mixing ratios in the gas phase. Systematic midday decreases in HCl* were not evident (Fig. 4). Indeed, during the two cleanest sampling

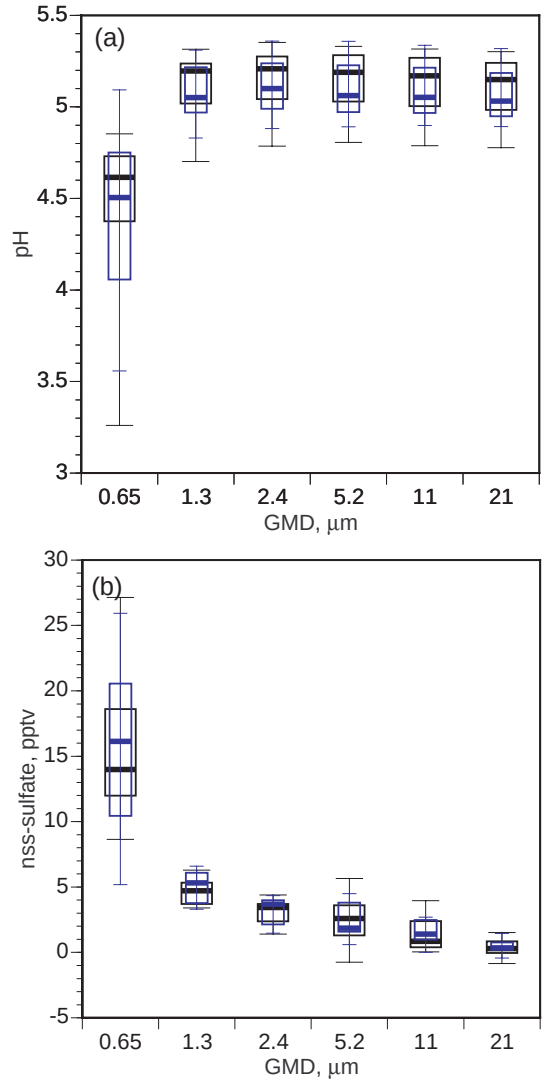

Fig. 2. Box-whisker plots of **(a)** aerosol pH during daytime (narrow blue boxes) and nighttime (wide black boxes) inferred from HCl phase partitioning, and **(b)** measured nss-SO_4^{2-} as a function of particle size. Box tops and bottoms indicate quartile values, whiskers indicate decile values, and thick horizontal bars indicate median values. Eleven daytime and eleven nighttime values were available for constructing each box.

periods (intensives 2 and 5, Table 2), HCl* mixing ratios peaked during midday (Fig. 4). These results suggest that the Laskin et al. (2003) mechanism of alkalinity production via surface reaction of OH with Cl^- in sea-salt aerosols did not affect S cycling appreciably under these clean marine conditions.

The $H^+ + SO_4^{2-} \rightleftharpoons HSO_4^-$ equilibrium resulted in most total acidity existing as HSO_4^- in all aerosol size fractions (Table 3, Saxena et al., 1993; Keene et al., 2002). Based on median values, total acidities were typically about 1.5 orders of magnitude greater than corresponding H^+ concentrations. In addition, all total acidities (expressed as $-\log_{10}[H^+_{tot}]$ or pH_t) for the four largest size fractions fell within a narrow range of 2.9 to 3.6 over the variable conditions observed during this experiment (Table 3). It is evident from Eq. (2) that at the high concentrations of SO_4^{2-} and low concentrations of H^+ that are typical of sea-salt aerosols (e.g. Table 3, Keene et al., 2002), the ratio $[HSO_4^-]/[H^+]$ is large and varies almost linearly with total $[SO_4^{2-}]$. Thus, the total acidity in sea-salt size fractions is determined in part by the total amount of SO_4^{2-} present. Based on median values for the four largest size fractions, sea-salt accounted for 94% of total SO_4^{2-} and sea-salt concentrations exhibited relatively little variability over the course of the experiment (Table 3). In addition RH varied within a fairly narrow range (Table 2) and, thus, water contents per unit sea-salt were similar across the super-μm size fractions (e.g. Gerber, 1985). Consequently, total $[SO_4^{2-}]$ and total acidity exhibited relatively little variability across the four largest size fractions during the course of the experiment. Although HSO_4^- represents a large fraction of total acidity in sea-salt aerosol solutions at Hawaii, absolute concentrations are low relative to the total amount of acidity in the entire multiphase system; gaseous acids (e.g. HCl) and sub-μm aerosol size fractions (Table 3) are the dominant reservoirs.

Equations (1) and (2) show that HCl mixing ratios and the sulphate equilibrium are directly coupled through H^+. For instance, combining and reorganising these expressions yields

$$\frac{HCl_g}{\{HSO_4^-\}} = \frac{\{Cl^-\}}{\{SO_4^{2-}\}} \times \frac{K_{aHSO_4^-}}{K_{aHCl} \times K_H}. \quad (3)$$

In all but the most polluted marine regions, Cl^- and SO_4^{2-} in sea-salt size fractions are present at concentrations close to sea-salt ratios and, consequently, the right side of the equation exhibits relatively little variability over the global MBL. Thus, the left side of the equation must also be relatively constant. This relationship provides useful context for comparing aerosol acidities across variable chemical regimes.

Median total acidities (expressed as pH_t) for the four largest size fractions at Hawaii (3.3 to 3.4, Table 3) were within the range of those observed in association with higher levels of pollutants at Bermuda (2.7 to 3.5, Keene et al., 2002). In contrast, the corresponding median H^+ activities (expressed as pH) at Hawaii (5.1 for all size fractions, Table 3) were less than those at Bermuda (4.1 to 4.6, Keene et al., 2002). As was the case at Hawaii, sea-salt accounted for most (93%) of total SO_4^{2-} in the four largest size fractions at Bermuda and corresponding median concentrations of total SO_4^{2-} (6.9 nmol m^{-3}, Keene et al., 2002) were similar to those at Hawaii (5.3 nmol m^{-3}). However, RHs at Bermuda (median=91% for the subset of samples with detectable acidities, Keene et al., 2002) were greater than those at Hawaii (Table 2). Consequently, aqueous concentrations of $[SO_4^{2-}]$, $[HSO_4^-]$, and corresponding equilibrium ratios of $[HSO_4^-]/[H^+]$ for detectable acidities at Bermuda were also

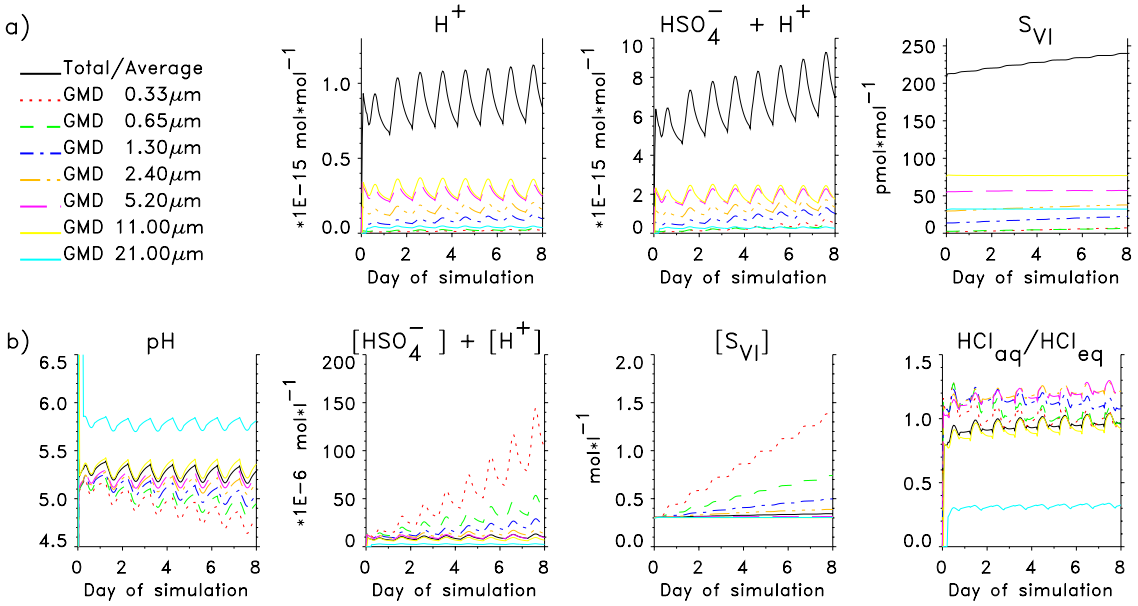

Fig. 3. Mixing ratios **(a)** and aqueous concentrations **(b)** in sea-salt aerosol simulated in M1. For HCl the ratio $[HCl]_{aq}/[HCl]_{eq}$ is shown, where the denominator is the equilibrium concentration with gas-phase HCl.

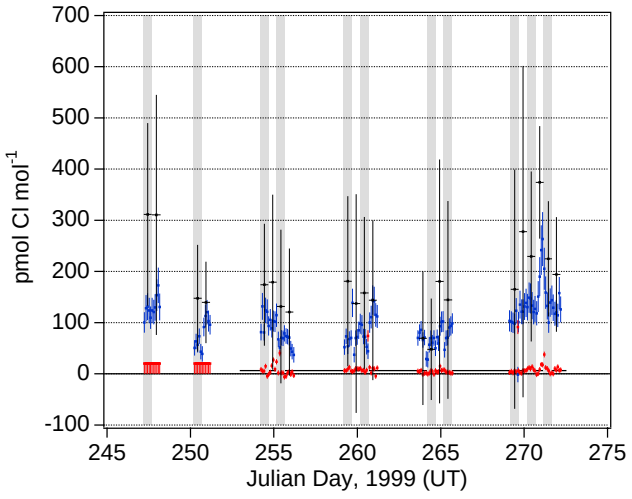

Fig. 4. Measured mixing ratios of HCl* (blue) and Cl* (red) and corresponding Cl^- deficits (black) summed over the impactor size fractions. All Cl* values were below a detection limit of about 20 pmol mol^{-1} during the first two intensive sampling periods. The lower detection limit of approximately 6 pmol mol^{-1} during the rest of the experiment is indicated by the thin black line drawn from JD 253 to JD 273. Error bars for HCl* and Cl* correspond to precisions stated in the text. For Cl^- deficits the horizontal error bars correspond to the sampling intervals and the vertical error bars represent the propagated precisions associated with the 14 individual measurements (7 Cl^- and 7 Mg^{2+}) underlying each sum. Shaded vertical bands indicate nighttime (sunset to sunrise) intervals during each intensive sampling period.

lower. The influences of higher solution $[H^+]$ and higher aerosol water content on $[HSO_4^-]$ at Bermuda relative to Hawaii were of comparable magnitude but opposite direction resulting in similar median total acidities in the four largest size fractions at the two sites. Although not measured at Bermuda during Spring 1997, we would predict from Eq. (3) that the corresponding HCl_g mixing ratios during that period were within the same range as those at Hawaii (Table 3). HCl_g mixing ratios under conditions of lower RH (79% to 93%) at Bermuda during Spring 1996 ranged from 133 to 883 pmol mol^{-1} (Keene and Savoie, 1998), which overlap the range of values at Hawaii.

Sea-salt aerosol pHs simulated by MOCCA were generally in agreement with those inferred from thermodynamic relationships with simulated values for most size fractions ranging between 4.9 and 5.5 (Fig. 3b). The corresponding range of pHs of super-μm size fractions inferred from thermodynamic relationships was 4.5 to 5.4 (Table 3). However, pHs for the largest size fraction in model simulations oscillated around a somewhat higher value of 5.9 due primarily to the rapid turnover rates and relatively larger infusions of alkalinity associated with fresh sea-salt aerosols. The constant production of new aerosols by wave action and the constant removal of reacted aerosols via deposition sustains dynamic disequilibria in both the model and in the ambient MBL. Larger size fractions have short lifetimes against deposition (in the model, 43, 18 and 8 h, respectively for particles with diameters 5.2, 11 and 21 μm). The corresponding times required to titrate sea-salt alkalinity and to acidify particles of these sizes to near equilibrium pHs were approximately 0.5, 2 and 6 h, respectively. For the largest size fraction, the

Table 3. Summary statistics for size-segregated aerosol composition at Hawaii during summer (N=22).

GMD μm	Statistic	LWC nL m^{-3}	Mg^{2+} nmol m^{-3}	EF(Cl)	EF(Br) nmol m^{-3}	NO_3^- nmol m^{-3}	NH_4^+ nmol m^{-3}	nss SO_4^{2-} nmol m^{-3}	HSO_4^- nmol m^{-3}	H^+ nmol m^{-3}	H_{tot} pH units	H^+
21.4	Max	2.66	2.50	1.02	1.08	0.19	0.04	0.07	1.5E-03	4.8E-05	1.5E-03	4.6
	Med	1.07	1.17	0.98	0.46	0.09	0.02	0.01	4.0E-04	7.8E-06	4.1E-04	5.1
	Min	0.43	0.43	0.91	<DL	<DL	<DL	<DL	1.7E-04	2.9E-06	1.7E-04	5.3
	Ave	1.18	1.27	0.97	0.45	0.10	0.02	0.02	5.2E-04	1.1E-05	5.3E-04	5.0
11.2	Max	7.48	7.54	1.02	0.65	1.44	0.04	0.22	4.0E-03	8.9E-05	4.0E-03	4.7
	Med	2.40	2.80	0.97	0.37	0.41	0.02	0.05	9.7E-04	1.7E-05	9.8E-04	5.1
	Min	0.84	1.06	0.91	<DL	0.13	<DL	<DL	3.2E-04	5.7E-06	3.3E-04	5.4
	Ave	2.76	3.11	0.94	0.32	0.53	0.02	0.06	1.3E-03	2.5E-05	1.3E-03	5.1
5.2	Max	5.62	6.00	0.98	0.44	4.22	0.05	0.28	3.1E-03	6.3E-05	3.1E-03	4.7
	Med	2.69	3.18	0.94	0.15	1.07	0.03	0.09	1.2E-03	2.2E-05	1.2E-03	5.1
	Min	1.36	1.57	0.80	<DL	0.43	0.01	<DL	4.6E-04	7.1E-06	4.7E-04	5.4
	Ave	2.82	3.41	0.93	0.18	1.23	0.03	0.10	1.4E-03	2.5E-05	1.4E-03	5.1
2.4	Max	2.29	2.60	0.96	0.40	2.02	0.07	0.19	1.4E-03	2.6E-05	1.4E-03	4.6
	Med	1.20	1.56	0.91	0.08	0.84	0.03	0.14	5.8E-04	9.3E-06	5.9E-04	5.1
	Min	0.49	0.55	0.70	<DL	0.33	0.01	0.02	1.7E-04	2.7E-06	1.7E-04	5.4
	Ave	1.18	1.51	0.90	0.08	0.88	0.03	0.13	6.5E-04	1.0E-05	6.6E-04	5.1
1.3	Max	1.20	1.40	0.90	1.13	1.06	0.09	0.29	1.4E-03	1.8E-05	1.4E-03	4.5
	Med	0.62	0.90	0.84	0.03	0.53	0.04	0.21	4.3E-04	5.2E-06	4.4E-04	5.1
	Min	0.23	0.26	0.54	<DL	0.20	0.02	0.13	1.4E-04	1.3E-06	1.4E-04	5.3
	Ave	0.62	0.80	0.82	0.08	0.54	0.04	0.20	5.1E-04	6.1E-06	5.1E-04	5.0
0.65	Max	1.11	1.73	0.96	1.43	1.07	1.73	1.27	2.1E-01	7.6E-04	2.1E-01	2.6
	Med	0.17	0.16	0.35	<DL	0.08	0.22	0.61	1.6E-03	5.2E-06	1.6E-03	4.6
	Min	0.08	0.04	0.02	<DL	0.02	0.02	0.09	3.3E-04	9.7E-07	3.3E-04	5.3
	Ave	0.22	0.22	0.45	<DL	0.25	0.36	0.65	1.7E-02	5.2E-05	1.7E-02	3.7
0.33	Max	0.62	0.33	8.1	27.	0.06	3.35	4.73	*	*	*	*
	Med	0.34	0.07	<DL	11.	<DL	0.45	2.88	*	*	*	*
	Min	0.12	<DL	<DL	<DL	<DL	<DL	1.23	*	*	*	*
	Ave	0.34	0.08	<DL	8.5	0.01	0.79	2.86	*	*	*	*
Sum	Max			0.96	0.56	8.96	4.53	6.32	*	*	*	*
	Med			0.93	0.33	3.30	0.82	4.08	*	*	*	*
	Min			0.77	0.05	1.22	0.21	2.01	*	*	*	*
	Ave			0.91	0.30	3.65	1.36	4.03	*	*	*	*
Bulk	Max			0.99	0.44	9.86	4.18	7.28	*	*	*	*
	Med			0.92	0.30	3.54	0.49	4.40	*	*	*	*
	Min			0.74	<DL	1.43	0.23	2.20	*	*	*	*
	Ave			0.91	0.27	3.95	0.83	4.40	*	*	*	*

Average Cl^- and Br^- enrichment factors based on average Mg^{2+} and average Cl^- and Br^-, respectively, for all samples.
$*$ Particulate Cl^- concentrations below detection limit; acidities and HSO_4^- cannot be inferred.

turnover rate and the rate of alkalinity titration are of similar magnitude and, consequently, the thermodynamic approach overestimates acidities of the largest particles.

The last panel in Fig. 3 depicts the equilibrium state of the modeled sea-salt particles with respect to HCl. From Eq. (1) the y-axis equals $\{H^+\}\times\{Cl^-\}/(\{H^+\}\times\{Cl^-\})_{eq}$. Because $\{Cl^-\}$ is many orders of magnitude larger than $\{H^+\}$, $\{Cl^-\}/\{Cl^-\}_{eq} \approx 1$ for the equilibrium in question and the ratio on the y-axis reflects variations in $\{H^+\}/\{H^+\}_{eq}$. The panel shows that $\{H^+\}$ in the largest size fraction was 3–5 times lower (0.5–0.7 pH unit) than the equilibrium value with respect to HCl. The size fractions with diameter 5.2 μm and smaller became slightly supersaturated and released HCl to the gas phase. Initially the supersaturation was larger

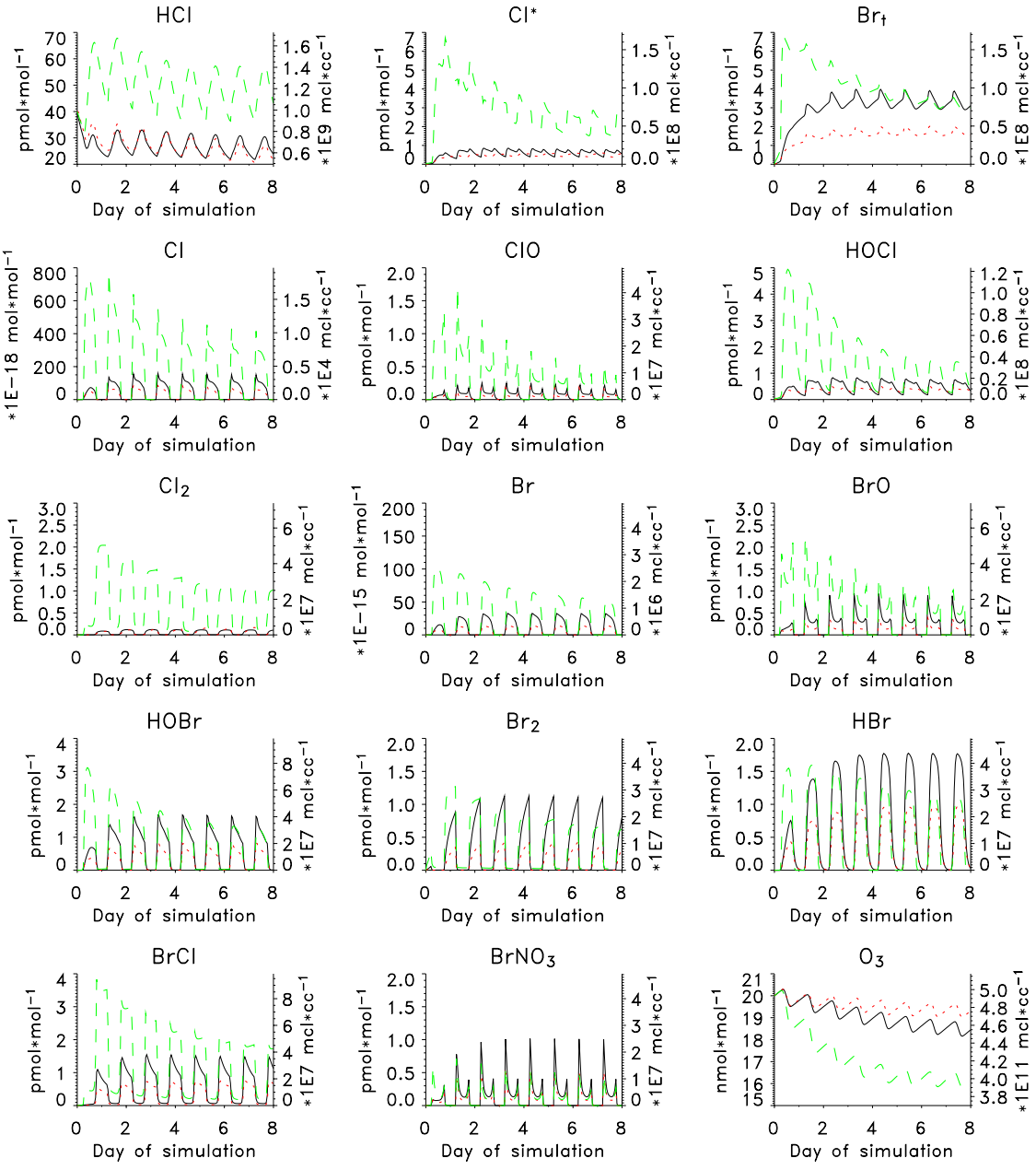

Fig. 5. Simulated mixing ratios of some halogen species and ozone in the gas phase in model runs M1 (black), M2 (red), and M3 (green).

for small particles because they absorb acids faster and because the ocean-atmosphere exchange process that introduces fresh, undersaturated sea-salt particles is slower. Acting in opposition to the absorption of acids is the halogen activation mechanism described by (R1) and (R2), which consumes acidity. Since the halogen cycling is more intensive in small particles, their supersaturation successively decreases relative to the larger particles and they even become undersaturated.

3.3 Halogen cycling

Measured mixing ratios of HCl* (primarily HCl) averaged 100 pmol mol^{-1} and varied from below detection limit (30 pmol mol^{-1}) to 250 pmol mol^{-1}; those of Cl* (Cl radicals, Cl_2, and HOCl) averaged 6 pmol mol^{-1} and varied from below detection limit (about 3 pmol mol^{-1} for most of the experiment) to 38 pmol mol^{-1} (Fig. 4). The maximum average mixing ratios of HCl* and Cl* over 12-hour periods (day- and nighttime) were 199 and 12 pmol mol^{-1}, respectively, and occurred during daytime. Based on all measurements,

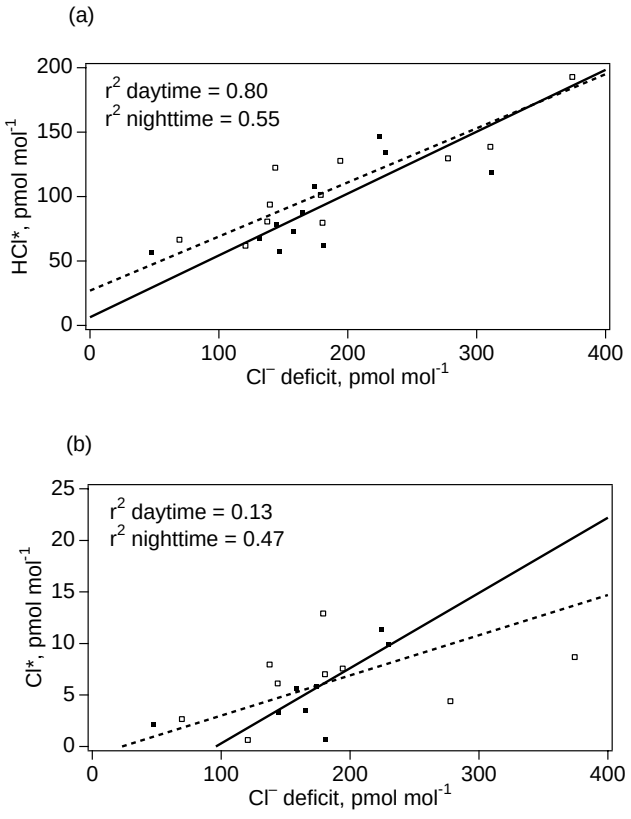

Fig. 6. Mixing ratios of HCl* **(a)** and Cl* **(b)** averaged over impactor sampling intervals plotted against corresponding measured particulate Cl^- deficits summed over all impactor stages (daytime: open squares; nighttime:solid squares). Lines are regressions for daytime (dashed) and nighttime (solid), respectively, calculated by the reduced major axis method (Hirsch and Gilroy, 1984). Regression coefficients: HCl* vs. Cl^- deficit daytime: slope=0.42, intercept=27; nighttime: slope=0.48, intercept=6.3; Cl* vs. Cl^- deficit daytime: slope=0.039, intercept=−0.9; nighttime: slope=0.073, intercept=−7.0.

mean mixing ratios of both HCl* and Cl* were slightly higher during daytime.

The simulated mixing ratios of HCl_g and Cl* varied between 20 and 70 pmol mol^{-1}, and 0.5 and 6 pmol mol^{-1}, respectively (Fig. 5), which are near the lower ends of the ranges of the respective measured concentrations. The higher mixing ratios during the latter part of the experiment were associated with the pollution episode and are not representative of the cleaner conditions considered in the simulations. The simulated HCl_g concentrations increased during the daytime, peaked before dusk, and decreased overnight to minimum values at dawn. Afternoon maxima in measured HCl* concentrations were observed on some days but a consistent diel pattern was not evident over the course of the experiment.

Simulated ClO, HOCl and Cl peaked during daytime while simulated Cl_2 peaked at night. The net effect is relatively little diel variability in simulated Cl* (Fig. 5). Absolute concentrations of simulated Cl* and associated diel patterns also differed among the cases studied. Simulation M1 indicated lower nighttime concentrations and an early morning minimum whereas simulation M3 indicated a nighttime maximum.

In the following discussion, particulate halogen "excesses" and "deficits" refer to absolute departure from sea water composition (i.e. nmol or pmol m^{-3}) while the terms "enrichment" and "depletion" refer to relative deviations. The measured particulate Cl^- deficits summed over all impactor stages do not show any clear diel variability (Fig. 4). The temporal variability over the course of the campaign resembled that of HCl* with larger deficits measured towards the end in association with high levels of pollutants. HCl* mixing ratios were strongly positively correlated to particulate Cl^- deficits during daytime and less strongly correlated at night, while correlations of Cl* mixing ratios to Cl^- deficits were weak or insignificant (Fig. 6).

The simulated Cl^- enrichments (EFCl= $(Cl^-/Mg^{2+})_{sample}/(Cl^-/Mg^{2+})_{seawater}$) in sea-salt particles were between 0.95 and 0.80, indicating Cl^- depletions similar to observed values. The Cl^- enrichment of sub-μm particles was between 0.75 and 0.25, indicating less Cl^- depletion than was observed; median measured enrichments were 0.35 and essentially zero for the 0.65 and 0.33 μm fractions, respectively (Table 3). This difference can be explained partly by the fact that the simulated sea-salt particles were externally mixed with sulphate particles at initialisation and did not physically mix during the model runs. They were therefore less acidic than actual sub-μm particles. The simulated diel pattern of the total (summed over all aerosol size fractions) Cl^- deficit showed a maximum rate of increase during afternoon and minimum at night (Fig. 7), which is consistent with diel variability indicated by the measurements (Fig. 4).

Mixing ratios of total gaseous inorganic Br (Br_t) varied from below detection limits (1.5–2 pmol mol^{-1}) to 9 pmol mol^{-1} (Fig. 8a) with average mixing ratio 3.7 pmol mol^{-1}. The maximum values were measured during daytime and the mean for mixing ratios during daytime was greater than that for nighttime. Mixing ratios also varied temporally over the course of the experiment in a similar way as Cl* (compare Fig. 4). The particulate Br^- deficit in bulk samples, expressed as mixing ratios, varied from 1 to 6 pmol mol^{-1} with average value 3.2 pmol mol^{-1}. Like Br_t, highest individual Br^- deficits and a higher mean deficit were measured during the daytime. The nighttime Br^- deficit data were positively correlated to Br_t while the daytime data were not (Fig. 9).

Maximum simulated mixing ratios of Br_t varied between 1.5 and 7.0 pmol mol^{-1} (Fig. 5), which are within the range of measured concentrations (Fig. 8). The higher values were associated with the higher concentrations of sea-salt particles in simulation M3. Maximum simulated mixing ratios of individual Br species (HBr, HOBr, BrO, BrCl, and Br_2 were

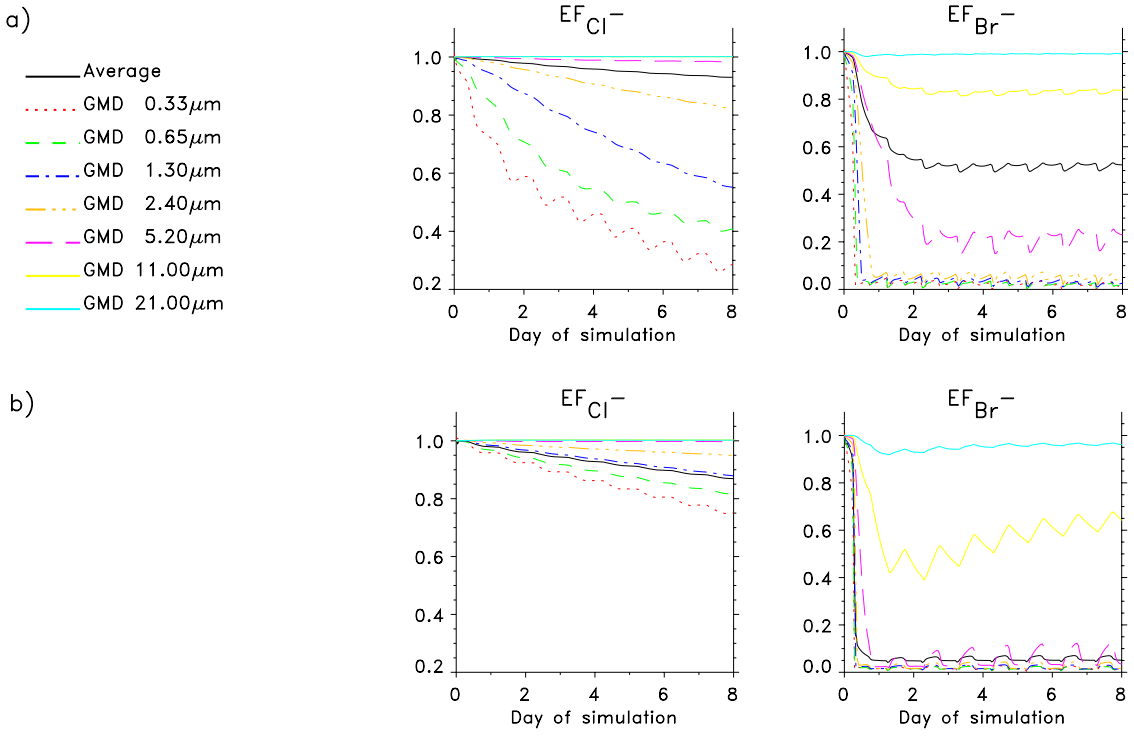

Fig. 7. Simulated concentrations of Cl^- and Br^- enrichment factors in sea-salt aerosols for model runs M1 **(a)** and M3 **(b)**.

each in the range of a few (1.5 to 3.0) pmol mol^{-1}; HBr, HOBr and BrO peaked during daytime and BrCl and Br_2 peaked at night. In all cases, Br_t mixing ratios were highest in the early morning and lowest at dusk. In simulations M1 and M2 the Br_t mixing ratio increased slowly overnight whereas, in simulation M3, the Br_t mixing ratio increased quickly after dusk. These differences account for higher average daytime mixing ratios of Br_t in simulations M1 and M2 compared to higher average nighttime mixing ratios in simulation M3. The diurnal variabilities of Br_t in the model are thus quite in agreement with measurements, with higher daytime Br_t mixing ratio on average but with some occasions when daytime mixing ratios were lower than those during the following night. Von Glasow et al. (2003) investigated the diurnal variability of Br_t with the 1-dimensional model MISTRA and found that presence of clouds influenced diurnal variability of Br_t. In simulations with clouds, Br_2 and BrCl, which would otherwise accumulate in the gas phase, dissolved into the cloud droplets causing nighttime minima in mixing ratios of these two compounds.

Diurnal variability in Br^- and EFBr also differed between simulations M1 and M2 relative to M3. Under the conditions of less intensive halogen cycling, the bromine volatilisation took place only during daytime when there were significant concentrations of HOBr driving the Br activation reaction R1. In simulation M2 no volatilisation took place at night and the EFBr increased due to the continuous air-sea exchange in the model replacing the bromine-depleted sea-salt particles with fresh ones. In simulations M1 and M3 with more intensive halogen cycling, larger gas phase mixing ratios of BrCl and Cl_2 developed after dusk and bromine volatilisation occurred as BrCl and Cl_2 dissolved into the sea-salt aerosol, volatilising Br_2. In M3 with slower air-sea exchange this nighttime volatilisation led to the lower nighttime mixing ratios of Br^- (and decreased EFBr) compared to daytime. In M1 with faster air-sea exchange the nighttime volatilisation was smaller than the relative increase of Br^- due to air-sea exchange, and the diurnal pattern was similar to that of simulation M2. Differences between diurnal variabilities in M1 and M3 can be seen in Fig. 7. The model results can be compared to the measured Br^- deficits (Fig. 8b) with slightly larger deficits during daytime than at night on average. Von Glasow and Crutzen (2003) recently compared diurnal cycles of Br^- in 1-D MISTRA model simulations with intensive and less intensive bromine volatilisation. They obtained opposite diurnal cycles in agreement with our simulations, however with much larger amplitude in a low Br^- volatilisation case. Rancher and Kritz (1980) reported diurnal variabilities of Br_t and Br^- over the equatorial Atlantic Ocean with consistently higher Br_t and lower Br^- during daytime.

Measured mixing ratios of BrO were less than detection limits of $\approx$2 pmol mol^{-1} throughout the experiment, which is consistent with model predictions (Fig. 5). To examine if a diel cycle in BrO can be discerned, data for changes in BrO mixing ratios over 3-hour periods, which generally have smaller uncertainties as noted above, were plotted over

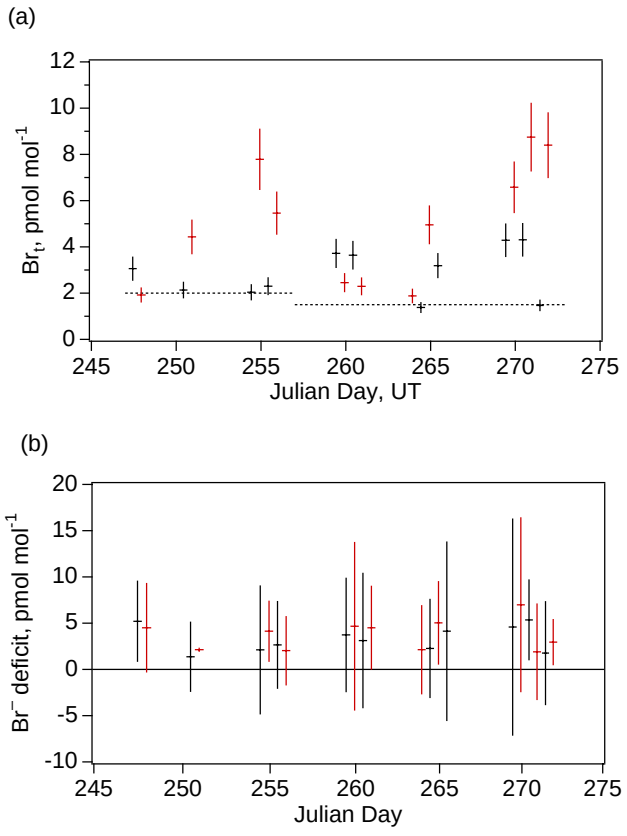

Fig. 8. Measured mixing ratios of **(a)** Br_t and **(b)** corresponding Br^- deficits in bulk aerosol during daytime (red) and nighttime (black); detection limits for Br_t are indicated with horizontal dashed lines in panel a. The widths of the red and black dash symbols correspond to the sampling intervals. Vertical error bars correspond to precisions stated in the text.

local time of the day (end of the 3-hour period) (Fig. 10). All data were lower than their respective detection limits, which reached as little as 0.5 pmol mol^{-1} when visibility was excellent. Only data with detection limits lower than 2 pmol mol^{-1} were considered. The data scattered around zero, however, changes in BrO mixing ratio during the 3-hour period ending at 11:00 local time were mostly negative, averaging -0.3 pmol mol^{-1}, which would be consistent with decreasing BrO mixing ratios during morning as simulated by MOCCA (Fig. 5). Evaluated BrO mixing ratios lower than the detection limit have to be taken with great care, as they may result from systematic features in the DOAS spectra, caused by diurnal changes of the lamp emission structures or by changes in trace gases absorbing in the wavelength region covered by the spectrum. Nonetheless, plots of changes of other trace gas concentrations as measured by DOAS do not show any noticeable diurnal variations, indicating that the uncertainty of the evaluation is mostly caused by random noise in the spectra.

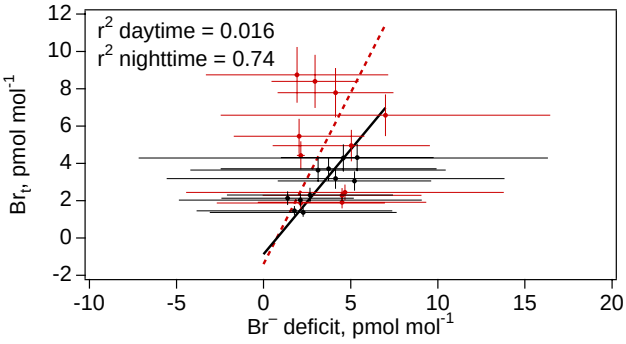

Fig. 9. Measured mixing ratios of Br_t versus corresponding Br^- deficits in bulk aerosol during the daytime (red) and nighttime (black). Error bars correspond to precisions stated in the text. Slanted lines are regressions for daytime (red dashed) and nighttime (black solid), respectively, calculated by the reduced major axis method (Hirsch and Gilroy, 1984). Regression parameters are as follows: Br_t vs. Br^- deficit daytime: slope=1.84, intercept=−1.40; Br_t vs. Br^- deficit nighttime: slope=1.12, intercept=−0.86.

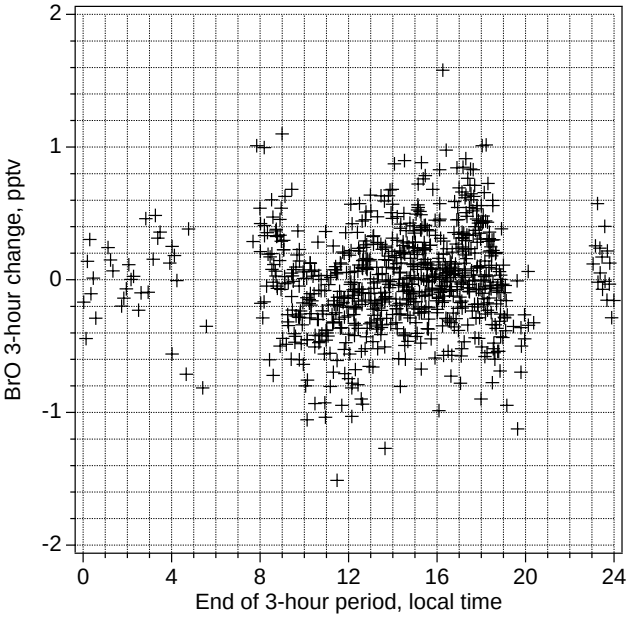

Fig. 10. Changes in BrO mixing ratios over a nominal 3-hour period plotted versus local time of end of the 3-hour period. Actual time differences between the two spectra used varied between 2.5 and 3.5 hours. All values were lower than their respective detection limits.

The measured Br^- concentrations and enrichments relative to sea salt indicate that most of the super-μm size fractions were depleted in Br^- (Table 3, Fig. 11). Bromide depletion increased with decreasing diameter from an average EF of about 0.5 for the >21 μm size fraction to 0.09 for the 2.4 μm size fraction. The 2.4 μm and 1.3 μm size fractions of most samples were almost completely depleted in Br^-. The smallest size fractions were typically enriched in Br^- relative to sea-salt (EFBr>1 for most of the samples).

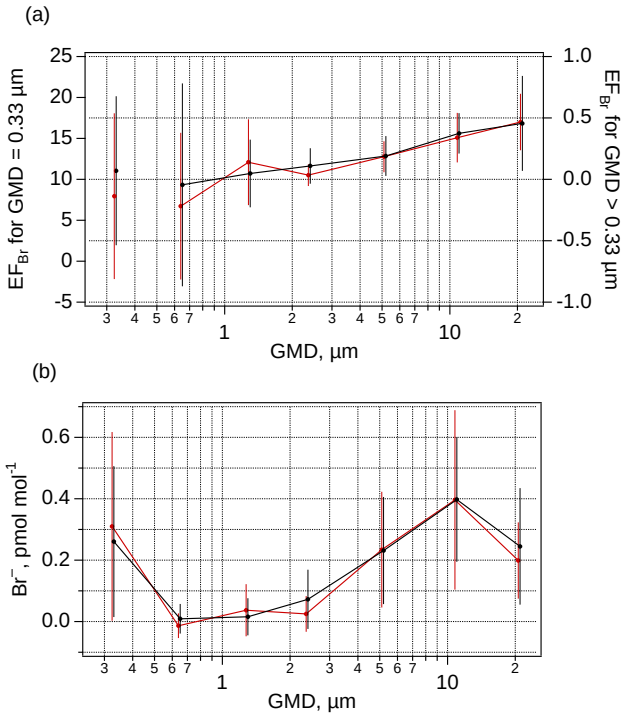

Fig. 11. Average particulate Br^- enrichment factors **(a)** and mixing ratios **(b)** as a function of size based on measured concentrations during daytime (red) and nighttime (black). Error bars are ± 1 standard deviation of the eleven values from which the averages were calculated for each point plotted. Daytime values are slightly offset horizontally to reduce overlap. Note the different scale for EFBr for the 0.33 μm size fraction in panel a.

The measured and simulated Br^- enrichments were comparable for most size fractions. Simulated enrichments integrated over all size fractions were between 0.6 and 0.9 and decreased from $\approx$0.95 in the largest particles to $\approx$0.05 in the 2.4 μm size bin (Figs. 7 and 11). However, the measured excess of Br^- in smallest size fraction (GMD 0.33 μm, Table 3) was not reproduced by the model. The simulated sub-μm sea-salt particles lost their bromine almost entirely. Externally mixed sulphate particles accumulated some bromine but this gain was at most 20 times less than the corresponding loss from similarly sized sea-salt particles.

Most of the measured particle mass in the sub-μm size fraction is contributed by SO_4^{2-}, NH_4^+ and associated H_2O (e.g. Table 2). These fine particles are also enriched in potassium and sometimes calcium relative to sea-salt, presumably due to terrestrial or combustion sources of K and Ca. Most sub-μm aerosols (or their surface layers) in the Hawaiian MBL are presumably hydrated and acidic so any associated Br^- should recycle, which makes it difficult to explain the enrichment by inorganic Br of non-marine origin. One possibility is that the Br^- is associated with chemically distinct particles, e.g. particles originating from combustion of leaded fuel in East-Asian vehicle fleets or particles originating from biomass burning. The highest Br^- enrichments were observed in association with the presence of significant pollutants, which trajectories suggest may have been transported from Asia. Alternatively, MOCCA may be missing some important process that leads to accumulation of sub-μm Br^-. See Sander et al. (2003) for further discussion of inorganic bromine chemistry in the MBL.

3.4 Interactions among halogens, ozone and nitrogen compounds

Sensitivity of the model to O_3 mixing ratio was explored. When the initial mixing ratio of O_3 was increased from 20 (simulation M1) to 30 nmol mol^{-1} (simulation M4), mixing ratios of reactive halogen species in the gas phase also increased (Fig. 12). Bromide depletions of sea-salt particles increased by up to 8%. Observed O_3 variations between 15 and 35 nmol mol^{-1} during the campaign may thus explain some of the variability in the measured halogen species. Gas-phase inorganic halogens reduce O_3 concentrations, making the sea-salt aerosol a catalytic reactor for O_3 destruction. This effect can be seen by comparing O_3 in simulations M2 and M3 (see Fig. 5). The O_3 mixing ratio at the end of simulation M3 with high sea-salt is 16 nmol mol^{-1} while in M2, with the lowest sea-salt mixing ratio, the O_3 mixing ratio is 19 nmol mol^{-1}. The $\approx$25% increase in sea-salt mixing ratio corresponds to a 16% O_3 decrease.

The role of the sea-salt particles in O_3 chemistry is rather complex. Ozone is destroyed catalytically by Br via reactions (R3) to (R5) and to some extent by the analogous Cl reactions. Reactions (R4) and (R5) convert HO_2 to OH, which also leads to O_3 destruction via the HO_x cycle:

$$OH + O_3 \rightarrow HO_2 + O_2 \quad \text{(R6)}$$

$$HO_2 + O_3 \rightarrow OH + 2O_2 \quad \text{(R7)}$$

These O_3 losses are partly offset by formation through reactions with NO

$$XO + NO \rightarrow X + NO_2 \quad (X=OH,\ Br,\ Cl) \quad \text{(R8)}$$

followed by NO_2 photolysis

$$NO_2 + h\nu \rightarrow NO + O. \quad \text{(R9)}$$

Ozone losses by various pathways were calculated in simulations M1 and M3 to quantify the effect of halogens on MBL O_3 concentration. In Fig. 13, the diel variation of O_3 loss due to (R3) plus its Cl analog is compared to losses due to O_3 photolysis and the HO_x and NO_x cycles. The contribution from (R8) was not subtracted from that of (R3) and was plotted separately because this reaction simultaneously contributes to O_3 formation in the NO_x cycle. Photolysis is the most important O_3 sink with a magnitude of approximately 1500 pmol O_3 mol^{-1} day^{-1}. In MOCCA this sink is approximately compensated by the stratospheric contribution. Figure 13 shows that the halogens deplete O_3 in the

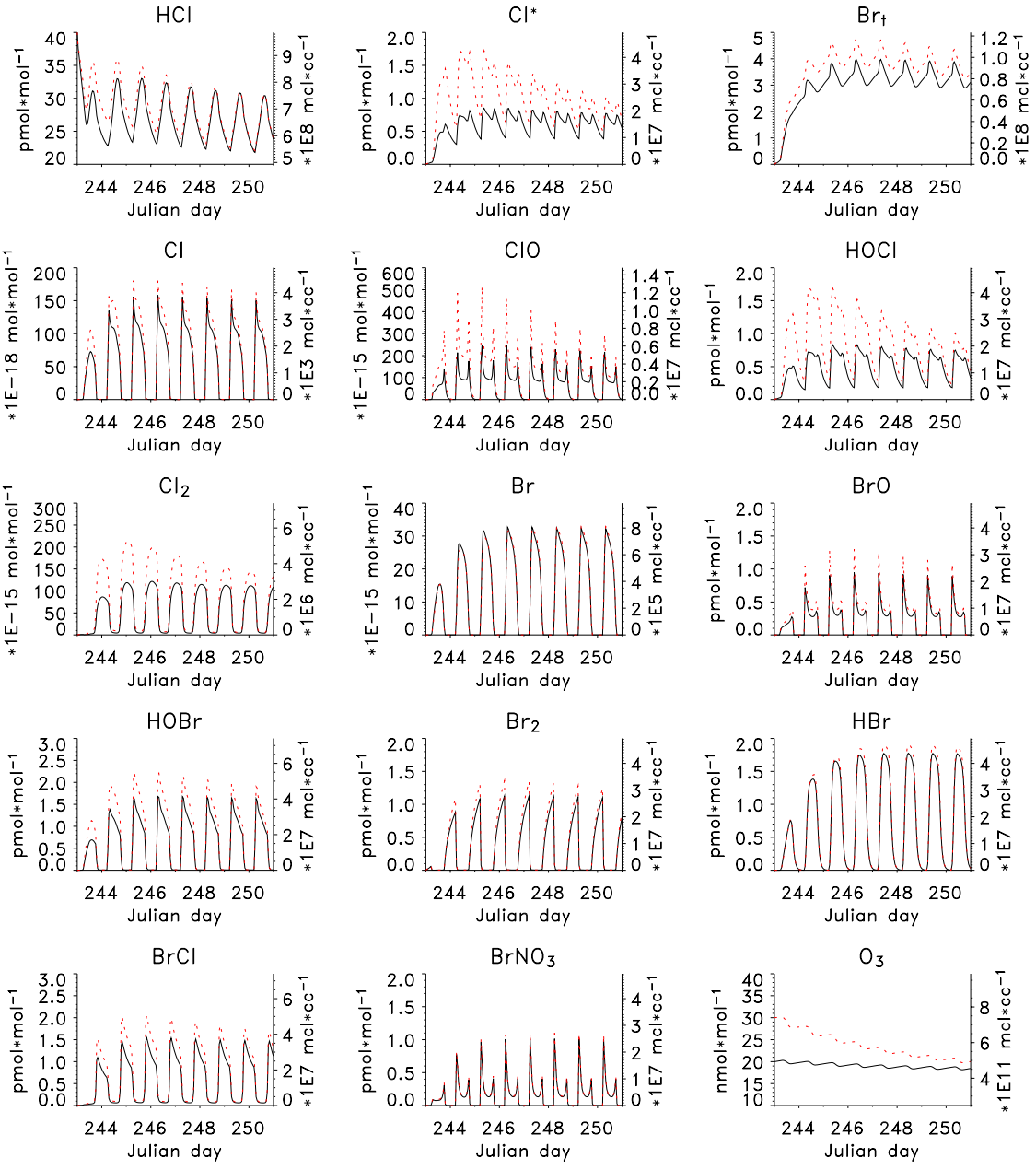

Fig. 12. Simulated mixing ratios of some halogen species and ozone in the gas phase in model runs M1 (black) and M4 (red, dotted).

MBL to an extent similar to that of the HO_x cycle (200 to 700 pmol mol^{-1} day^{-1}). Increasing sea-salt aerosol concentration (and particle surface area) from that in simulation M1 to that in M3, increases O_3 depletion by approximately a factor of two. Dry deposition of O_3 to the sea surface was of similar magnitude to that of the HO_x-cycle sink in both simulations. At the same time, photochemical O_3 formation decreased by a factor of 2 from 1540 to 790 pmol mol^{-1} day^{-1} at the beginning of simulation M3. This decrease was caused by more intensive removal of NO_x from the gas phase, which was mainly caused by heterogeneous reaction of $BrNO_3$ with sea-salt particles. It is the coupling between NO_x and halogen cycles that makes the sea-salt – O_3 interaction complex. Halogen nitrates are formed through

$$XO + NO_2 \rightarrow XNO_3 \ (X=Br,\ Cl). \qquad \text{(R10)}$$

In the model these nitrates react with liquid aerosols (Sander et al., 1999):

$$XNO_3 + H_2O_{(l)} \rightarrow HOX + HNO_3 \qquad \text{(R11)}$$

$$XNO_3 + X^- \rightarrow X_2 + NO_3^- . \qquad \text{(R12)}$$

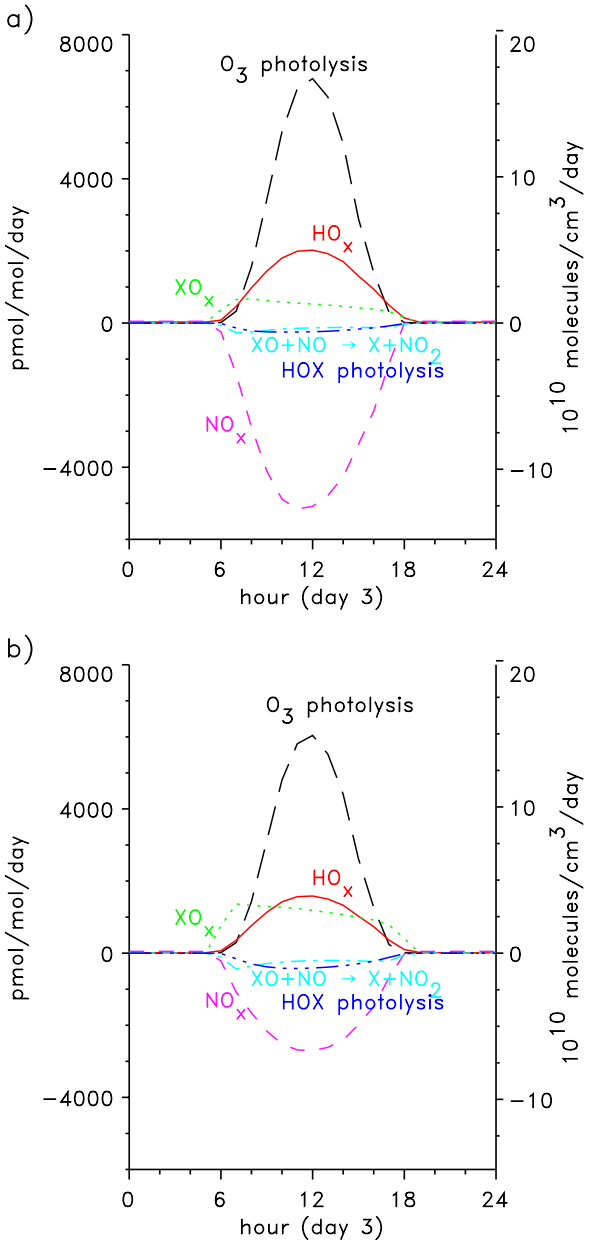

Fig. 13. Diel cycles of different ozone sinks from simulations M1 **(a)** and M3 **(b)**. Negative values imply net ozone production.

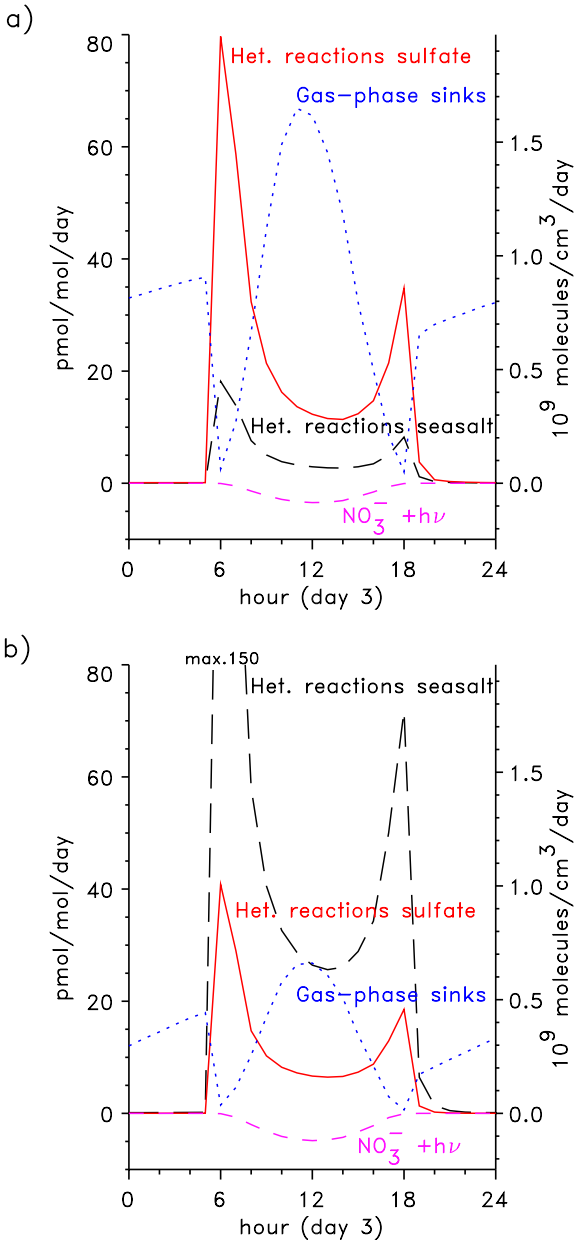

Fig. 14. Diel cycles of different sinks of NO_x from simulations M1 **(a)** and M3 **(b)**. Negative values are sources from NO_3^- photolytic reduction in sea-salt particles.

Nitric acid can be reduced to NO_2 in the gas phase by photolysis and by reaction with OH. In the aqueous phase, NO_3^- can be photolysed to NO_2 and OH.

The budgets of different NO_x sinks are compared in Fig. 14. The gas-phase sinks were mainly reaction of NO_2 with OH (55 to 60%) and reaction of DMS with NO_3. Gas-phase reduction of HNO_3 to NO_2 was unimportant in both model simulations (0.2 pmol mol^{-1} day^{-1} in maximum). The heterogeneous sink of NO_2 (R10) was followed by (R11) or (R12) with $BrNO_3$ responsible for 80 to 95% of the integrated 24-hour loss of NO_x through (R10) to (R12). On sea-salt particles the most important heterogeneous reaction of $BrNO_3$ was reaction with Cl^- while on the sulphate particles it was hydration. In sea-salt particles a few pmol mol^{-1} day^{-1} of NO_3^- were reduced back to NO_2 through photolysis. This reaction was negligible in sulphate particles.

In Fig. 14 it is shown that in M1 (low sea-salt) the gas-phase reactions were the most important sink of NO_x, although heterogeneous reactions with sulphate particles were responsible for approximately 25% of the total loss of NO_x. The sulphate particles did not retain the NO_3^- formed in (R11) and (R12). HCl scavenged to the particles provided Cl^- to (R12) to form BrCl and the associated acidity repartitioned the HNO_3 to the gas phase. In this way the sulphate particles in the model were effective both in removing NO_x and re-activating chlorine. In contrast, the sea-salt particles in the model retained the NO_3^- formed through (R11) and (R12). After three days of simulation the mixing ratio of NO_3^- in aerosol particles reached approximately 100 pmol mol^{-1}, which is rather close to the mean measured mixing ratio (e.g. Table 3). In simulation M1 the heterogeneous sink of NO_x on sea-salt particles was approximately 5% of the total. In simulation M3 with higher sea-salt concentration (but the same nss sulphate concentration) the importance of reactions of $BrNO_3$ with sea-salt particles as a sink for NO_x increased greatly and became the most important, accounting for as much as 60% of the removal. The photolytic reduction of NO_3^- in sea-salt particles increased by about 1.4 pmol mol^{-1} day^{-1} as a result of these reactions, thereby reducing the net magnitude of this sink by 0.5 to 2.5%.

The accommodation coefficient of $BrNO_3$ is rather uncertain. To test the sensitivity of the model in this regard the sticking coefficient of $BrNO_3$ was decreased from 0.8 (used in simulations M1 to M4) to 0.1 and 0.01. The effects on oxides of nitrogen were approximately +2 and +5 pmol mol^{-1}, respectively, and on inorganic volatile bromine 0 and -1 pmol mol^{-1}, respectively. Comparison of the high- and low-sticking coefficient simulations indicates that the additional oxides of nitrogen were to a large extent missing from the sea-salt particles' nitrate pool, illustrating the complexity of cycling of species through these particles.

It was not possible to directly estimate from the model the response of O_3 to the removal of NO_x through heterogeneous reactions of $BrNO_3$ and $ClNO_3$. However, the difference in O_3 formation between M1 and M3 was 700 to 900 pmol mol^{-1} day^{-1} during the initial day of simulation while the catalytic O_3 destruction by the Br-BrO and Cl-ClO cycles increased by 300 to 600 pmol mol^{-1} day^{-1}. The total O_3 response was -1.0 to -1.5 nmol mol^{-1} day^{-1}, a range similar to the total O_3 sink by photolysis in both simulations.

4 Conclusions

A multiphase suite of inorganic Cl and Br species and related chemical and physical parameters was measured in the relatively clean easterly trade-wind regime over the North Pacific Ocean at Hawaii during September 1999. Aerosols were sampled over 11 diel cycles with cascade impactors and bulk filters, which were analysed for ionic composition. Volatile inorganic Cl gases were sampled with tandem mist chambers to segregate HCl* (primarily HCl) and Cl* (including Cl_2 and HOCl) fractions. BrO, NO_2 and O_3 were measured with a long-path DOAS. Total gaseous inorganic Br was sampled with alkaline-impregnated filters.

Aerosol pH as a function of particle size was inferred from the measured phase partitioning and thermodynamic properties of HCl. The photochemical box model MOCCA was parameterized based on observations and the measured concentrations and calculated results were compared with simulations over a representative range of conditions.

Aerosol pHs inferred from measured phase partitioning were acidic for all aerosol size fractions, with those for super-μm ranging from the 4.5 to 5.4 (median 5.1). The sub-μm fraction (GMD 0.65 μm) acidities were higher (median pH 4.6) and more variable. Inferred daytime pHs tended to be slightly lower than those at night, although daytime median values did not differ statistically from nighttime medians. pHs predicted by MOCCA were generally in agreement with those inferred from thermodynamic relationships: 4.9 to 5.5 for super-μm fractions and 5.3 to 5.5 for sub-μm fractions. These differences are probably due to the simulations representing a relatively clean subset of the conditions sampled and, for the largest particles, due to the rapid turnover rates and relatively larger infusions of sea-salt alkalinity associated with fresh aerosols. The simulation-based pHs should therefore be considered upper limits.

Measured mixing ratios of HCl* ranged from <30 to 250 pmol mol^{-1} and those for Cl* from <6 to 38 pmol mol^{-1}. Afternoon HCl* maxima were observed on some days but not on others. A consistent diel variation pattern for HCl* or Cl* was not observed. Simulated HCl and Cl* ($Cl + ClO + HOCl + Cl_2$) mixing ratios ranged between 20 and 70 pmol mol^{-1} and 0.5 and 6 pmol mol^{-1}, respectively, both of which were within the ranges of measured values. While individual components of Cl* varied diurnally in the simulations, their sum did not, consistent with the lack of a diel cycle in observed Cl*. Simulated HCl did vary diurnally, peaking before dusk and reaching a minimum at dawn, in agreement with HCl* observations on some days but not on others.

Mixing ratios of alkaline-reactive Br varied from <1.5 to 9 pmol mol^{-1} with values tending to be higher during daytime. Particulate Br deficits varied from 1 to 6 pmol mol^{-1} with the greatest deficits also tending to occur during daytime. Simulated Br_t and Br^- mixing ratios and EFBr values were similar to those observed with early morning maxima and dusk minima. However, the diel cycles differed in detail among the various simulations. In low-salt simulations halogen cycling was less intense, Br^- accumulated and Br_t and EFBr increased slowly overnight. In higher-salt simulations with more intense halogen cycling Br^- and EFBr decreased and Br_t increased rapidly after dusk. Cloud processing, which is not considered in this version of MOCCA, may also affect these diel cycles (von Glasow

and Crutzen, 2003). Measured BrO was never above detection limit ($\approx$2 pmol mol^{-1}) during the experiment, however relative changes in the BrO signal during the 3-hour period ending at 11:00 local time were mostly negative, averaging -0.3 pmol mol^{-1}. Both of these results are consistent with MOCCA simulations of BrO mixing ratios.

The impact of multiphase halogen cycling on O_3 was explored by initialising the MOCCA model with different O_3 mixing ratios and sea-salt aerosol concentrations within the ranges of observed values. Increasing sea-salt mixing ratio by $\approx$25% led to a decrease in O_3 of $\approx$16%. The chemistry leading to this decrease is complex and is tied to NO_x removal by heterogeneous reactions of $BrNO_3$ and $ClNO_3$. The sink of O_3 due to the catalytic X-XO cycles is estimated at -1.0 to -1.5 nmol mol^{-1} day^{-1}, a range similar to that due to O_3 photolysis in the MOCCA simulations.

Acknowledgements. We thank C. Adams-Phillips, S. Howell and B. Huebert of the University of Hawaii for use of the tower facility and operational support during the field campaign at Bellows Air Force Station. G. Kleiman assisted in calculating trajectories at MIT. Funding for this work was provided by the German BMBF's program AFO 2000, the U.S. National Science Foundation through award ATM-0003865 to UVA, and the U.S. National Oceanic and Atmospheric Administration through contract NA87RJ0445 to MIT via the Cooperative Institute for Climate and Ocean Research at the Woods Hole Oceanographic Institution.

References

Ayers, G. P., Gillett, R. W., Cainey, J. M., and Dick, A. L.: Chloride and bromide loss from sea-salt particles in the southern ocean air, J. Atmos. Chem., 33, 299–319, 1999.

Bardwell, C. A., Maben, J. R., Hurt, J. A., Keene, W. C., Galloway, J. N., Boatman, J. F., and Wellman, D.: A technique using high-flow, dichotomous filter packs for measuring major atmospheric chemical constituents, Global Biogeochem. Cycles, 4, 151–163, 1990.

Bass, A. M. and Paur, R. J.: The ultraviolet cross-sections of ozone, Proceedings of the Quadrennial Ozone Symposium, Greece (edited by Zerefos, C. and Ghazi, A.), 60 6617, 1984.

Brauers, T., Hausmann, M., Brandenburger, U., and Dorn, H.-P.: Improvement of differential optical absorption spectroscopy with a multichannel scanning technique, Appl. Opt., 34, 4472–4479, 1995.

Brimblecombe, P. and Clegg, S. L.: Erratum, J. Atmos. Chem., 8, 95, 1989.

Chameides, W. L. and Stelson, A. W.: Aqueous-phase chemical processes in deliquescent sea salt aerosols: A mechanism that couples the atmospheric cycles of S and sea salt, J. Geophys. Res., 97, 20 565–20 580, 1992.

Cicerone, R. J.: Halogens in the troposphere, Rev. Geophys., 19, 123–139, 1981.

Clegg, S. L. and Whitfeldt, M.: Activity coefficients in natural waters, in Pitzer, K. S., Activity Coefficients in Electrolyte Solutions, CRC Press, Boca Raton, FL, 279–434, 1991.

Dickerson, R. R., Rhodes, K. P., Carsey, T. P., Oltmans, S. J., Burrows, J. P., and Crutzen, P. J.: Ozone in the remote marine boundary layer: A possible role for halogens, J. Geophys. Res., 104, 21 385–21 395, 1999.

Draxler, R. R.: HYbrid Single-Particle Lagrangian Integrated Trajectories (HY-SPLIT): Version 3.0-User's guide and model description, NOAA Tech. Memo. ERL/ARL-80, 40, 1995.

Erickson III, D. J., Seuzaret, C., Keene, W. C., and Gong, S.-L.: A general circulation model based calculation of HCl and $ClNO_2$ production from sea salt dechlorination: Reactive Chlorine Emissions Inventory, J. Geophys. Res., 104, 8347–8372, 1999.

Galbally, I. E., Bentley, S. T., and Meyer, C. P.: Mid-latitude marine boundary-layer ozone destruction at visible sunrise observed at Cape Grim, Tasmania, Geophys. Res. Lett., 27, 3841–3844, 2000.

Gerber, H. E.: Relative-humidity parameterization of the Navy aerosol model (NAM), NRL Rep. 8956, Naval Res. Lab., Washington, D. C., 1985.

Gong, S. L., Barrie, L. A., and Blanchet, J.-P.: Modeling sea-salt aerosols in the atmosphere: 1. Model Development, J. Geophys. Res., 102, 3805–3818, 1997.

Graedel, T. E. and Keene, W. C.: The tropospheric budget of reactive chlorine, Global Biogeochem. Cycles, 9, 47–78, 1995.

Harder, J. W., Brault, J. W., Johnston, P. V., and Mount, G. H.: Temperature dependent NO_2 cross sections at high spectral resolution, J. Geophys. Res., 102, 3861–3879, 1997.

Hebestreit, R. M., Stutz, J., Rosen, D., Matveev, V., Luria, M., and Platt, U.: DOAS measurements of tropospheric bromine oxide in mid-latitudes, Science, 283, 55–57, 1999.

Hirsch, R. M. and Gilroy, E. J.: Methods of fitting a straight line to data: Examples in water resources, Water. Resour. Bull., 20, 5, 705–711, 1984.

Hönninger, G.: Referenzspektren reaktiver Halogenverbindungen für DOAS-Messungen, Diplomarbeit, Ruprecht-Karls-Universität Heidelberg, Germany, http://www.iup.uni-heidelberg.de/urmel/abstracts/tit2hg.html, 1999.

Jobson, B. T., Niki, H., Yokouchi, Y., Bottenheim, J., Hopper, F., and Leaitch, R.: Measurements of C_2-C_6 hydrocarbons during the Polar Sunrise 1992 Experiment: Evidence for Cl atom and Br atom chemistry, J. Geophys. Res., 99, 25 355–25 368, 1994.

Jobson B. T., Parrish, D. D., Goldan, P., Kuster, W., Fehsenfeld, F. C., Blake, D. R., Blake, N. J., and Niki, H.: Spatial and temporal variability of nonmethane hydrocarbon mixing ratios and their relation to photochemical lifetime, J. Geophys. Res., 103, 13 557–13 567, 1998.

Keene, W. C. and Savoie, D. L.: The pH of deliquesced sea-salt aerosol in polluted marine air. Geophys. Res. Lett., 25, 2181–2184, 1998.

Keene, W. C. and Savoie, D. L.: Correction to "The pH of deliquesced sea-salt aerosol in polluted marine air", Geophys. Res. Lett., 26, 1315–1316, 1999.

Keene, W. C., Pszenny, A. A. P., Galloway, J. N., and Hawley, M. E.: Sea-salt corrections and interpretation of constituent ratios in marine precipitation, J. Geophys. Res., 91, 6647–6658, 1986.

Keene, W. C., Talbot, R. W., Andreae, M. O., Beecher, K., Berresheim, H., Castro, M., Farmer, J. C., Galloway, J. N., Hoffman, M. R., Li, .S.-M., Maben, J. R., Munger, J. W., Norton, R. B., Pszenny, A. A. P., Puxbaum, H., Westberg, H., and Winiwarter, W.: An intercomparison of measurement systems for vapor- and particulate-phase concentrations of formic and acetic

acids, J. Geophys. Res., 94, 6457–6471, 1989.
Keene, W. C., Pszenny, A. A. P., Jacob, D. J., Duce, R. A., Galloway, J. N., Schultz-Tokos, J. J., Sievering, H., and Boatman, J. F.: The geochemical cycling of reactive chlorine through the marine troposphere, Global Biogeochem. Cycles, 4, 407–430, 1990.
Keene, W. C., Maben, J. R., Pszenny, A. A. P., and Galloway, J. N.: Measurement technique for inorganic chlorine gases in the marine boundary layer, Environ. Sci. Technol., 27, 866–874, 1993.
Keene, W. C., Sander, R., Pszenny, A. A. P., Vogt, R., Crutzen, P. J., and Galloway, J. N.: Aerosol pH in the marine boundary layer: A review and model evaluation, J. Aerosol Sci., 29, 339–356, 1998.
Keene, W. C., Pszenny, A. A. P., Maben, J. R., and Sander, R.: Variation of marine aerosol acidity with particle size, Geophys. Res. Lett., 29, 7, 10.1029/2001GL013881, 2002.
Laskin, A., Gaspar, D. J., Wang, W., Sherri, W., Hunt, S. W., Cowin, J. P., Colson, S. D., and Finlayson-Pitts, B. J.: Reactions at interfaces as a source of sulfate formation in sea salt particles, Science, 301, 340–344, 2003.
Laszlo, B., Kurylo, M. J., and Huie, R. E.: Absorption cross sections, kinetics of formation, and self-reaction of the IO radical produced via laser photolysis of $N_2O/I_2/N_2$ mixtures, J. Phys. Chem., 99, 11 701–11 707, 1995.
Leser, H., Hönninger, G., and Platt, U.: MAX-DOAS measurements of BrO and NO_2 in the marine boundary layer, Geophys. Res. Lett., 30, 10, 10.1029/2002GL015811, 2003.
Li, S. M., Yokouchi, Y., Barrie, L. A., Muthuramu, K., Shepson, P. B., Bottenheim, J. W., Sturges, W. T., and Landsberger, S.: Organic and inorganic bromine compounds and their composition in the Arctic troposphere during polar sunrise, J. Geophys. Res., 99, 25 415–25 428, 1994.
Maben, J. R., Keene, W. C., Pszenny, A. A. P., and Galloway, J. N.: Volatile inorganic chlorine in surface air over eastern North America, Geophys. Res. Lett., 22, 3513–3516, 1995.
Marsh, A. R. W. and McElroy, W. J.: The dissociation constant and Henry's law constant of HCl in aqueous solution, Atmos. Environ., 19, 1075–1080, 1985.
Martinez, M., Arnold, T., and Perner, D.: The role of bromine and chlorine chemistry for arctic ozone depletion events in Ny Ålesund and comparison with model calculations, Ann. Geophys., 17, 941–956, 1999.
Martinez, M., Perner, D., Hackenthal, E.-M., Külzer, S., and Schütz, L.: Measurements of NO_3 at Helgoland during the NORDEX campaign in October 1996, J. Geophys. Res., 105, 22 685–22 695, 2000.
McFiggans, G., Allan, B., Coe, H., Plane, J. M. C., Carpenter, L. J., and O'Dowd, C.: A modeling study of iodine chemistry in the marine boundary layer, J. Geophys. Res., 105, 14 371–14 385, 2000.
Meng, Z. and Seinfeld, J. H.: Time scales to achieve atmospheric gas-aerosol equilibrium for volatile species, Atmos. Environ., 30, 2889–2900, 1996.
Mozurkewich, M.: Mechanisms for the release of halogens from sea-salt particles by free radical reactions, J. Geophys. Res., 100, 14 199–14 207, 1995.
O'Dowd, C. D., Jimenez, J. L., Bahreini, R., Flagan, R. C., Seinfeld, J. H., Hameri, K., Pirjola, L., Kulmala, M., Jennings, S. G., and Hoffmann, T.: Marine aerosol formation from biogenic iodine emissions, Nature, 417, 632–636, 2002.
Parrish, D. D., Hahn, C. J., Williams, E. J., Norton, R. B., Fehsenfeld, F. C., Singh, H. B., Shetter, J. D., Gandrud, B. W., and Ridley, B. A.: Reply to comment on "Indications of photochemical histories of Pacific air masses from measurements of atmospheric trace gases at Pt. Arena, California", J. Geophys, Res., 98, 14 995–14 997, 1993.
Pitzer, K. S.: Activity Coefficients in Electrolyte Solutions, CRC Press, Boca Raton, FL, 1991.
Platt, U.: Differential optical absorption spectroscopy (DOAS), In: Air monitoring by spectroscopic techniques, M. W. Sigrist, Ed., Chemical Analysis Series, 127, John Wiley & Sons, 1994.
Platt, U. and Perner, D.: Measurements of atmospheric trace gases by long path differential UV/visible absorption spectroscopy, Optical and Laser Remote Sensing (edited by D. K. Killinger and A. Mooradien), Springer Ser. Optical Sci., 39, 95–105, 1983.
Pszenny, A. A. P., Castelle, A. J., Galloway, J. N., and Duce, R. A.: A study of the sulfur cycle in the Antarctic marine boundary layer, J. Geophys. Res., 94, 9818–9830, 1989.
Pszenny, A. A. P., Keene, W. C., Jacob, D. J., Fan, S., Maben, J. R., Zetwo, M. P., Springer-Young, M., and Galloway, J. N.: Evidence of inorganic chlorine gases other than hydrogen chloride in marine surface air, Geophys. Res. Lett., 20, 699–702, 1993.
Rancher, J. and Kritz, M. A.: Diurnal fluctuation of Br and I in the marine atmosphere, J. Geophys. Res., 85, 5581–5587, 1980.
Sander, R.: Compilation of Henry's law constants for inorganic and organic species of potential importance in environmental chemistry, version 3, http://www.mpch-mainz.mpg.de/~sander/res/henry.html, 1999.
Sander, R. and Crutzen, P. J.: Model study indicating halogen activation and ozone destruction in polluted air masses transported to sea, J. Geophys. Res., 101, 9121–9138, 1996.
Sander, R., Rudich, Y., von Glasow, R., and Crutzen, P. J.: The role of $BrNO_3$ in marine tropospheric chemistry: A model study, Geophys. Res. Lett., 26, 2858–2860, 1999.
Sander, R., Keene, W. C., Pszenny, A. A. P., Arimoto, R., Ayers, G. P., Baboukas, E., Cainey, J. M., Crutzen, P. J., Duce, R. A., Hönninger, G., Huebert, B. J., Maenhaut, W., Mihalopoulos, N., Turekian, V. C., and van Dingenen, R.: Inorganic bromine in the marine boundary layer: A critical review, Atmos. Chem. Phys., 3, 1301–1336, 2003.
Saxena, P., Mueller, P. K., Kim, Y. P., Seinfeld, J. H., and Koutrakis, P.: Coupling thermodynamic theory with measurements to characterize acidity of atmospheric particles, Aerosol Sci. Technol., 19, 279–293, 1993.
Singh, H. B., Gregory, G. L., Anderson, B., Browell, E., Sachse, G. W., Davis, D. D., Crawford, J., Bradshaw, J. D., Talbot, R., Blake, D. R., Thornton, D., Newell, R., and Merrill, J.: Low ozone in the marine boundary layer of the tropical Pacific Ocean: Photochemical loss, chlorine atoms, and entrainment, J. Geophys. Res., 101, 1907–1917, 1996a.
Singh, H. B., Thakur, A. N., and Chen, Y. E.: Tetrachloroethylene as an indicator of low Cl atom concentrations in the troposphere, Geophys. Res. Lett., 23, 1529–1532, 1996b.
Slinn, S. A. and Slinn, W. G. N.: Predictions for particle deposition on natural waters, Atmos. Environ., 14, 1013–1016, 1980.
Spicer, C. W., Chapman, E. G., Finlayson-Pitts, B. J., Plastridge, R. A., Hubbe, J. M., Fast, J. D., and Berkowitz, C. M.: Observations of molecular chlorine in coastal air, Nature, 394, 355–356, 1998.
Stutz, J. and Platt, U.: Numerical analysis and estimation of the statistical error of differential optical absorption spectroscopy

measurements with least-squares methods, Appl. Opt., 35, 6041, 1996.

Tanaka, P. L., Oldfield, S., Neece, J. D., Mullins, C. B., and Allen, D. T.: Anthropogenic sources of chlorine and ozone formation in urban atmospheres, Environ. Sci. Technol., 34, 4470–4473, 2000.

Tang, I. N.: Thermodynamic and optical properties of mixed-salt aerosols of atmospheric importance, J. Geophys. Res., 102, 1883–1893, 1997.

Tang, I. N. and Munkelwitz, H. R.: Water activities, densities, and refractive indices of aqueous sulphates and sodium nitrate droplets of atmospheric importance, J. Geophys. Res., 99, 18 801–18 808, 1994.

Vogt, R., Crutzen, P. J., and Sander, R.: A mechanism for halogen release from sea-salt aerosol in the remote marine boundary layer, Nature, 383, 327–330, 1996.

Von Glasow, R. and Crutzen, P. J.: Model study of multiphase DMS oxidation with a focus on halogens, Atmos. Chem. Phys. Discuss., 3, 6733-6777, 2003.

Von Glasow, R., Sander, R., Bott, A., and Crutzen, P. J.: Modeling halogen chemistry in marine boundary layer 2. Interactions with sulfur and the cloud-covered MBL, J. Geophys. Res., 107, 4323, doi:10.1029/2001JD000943, 2002.

Wagner, T. and Platt, U.: Satellite mapping of enhanced BrO concentration in the troposphere, Nature, 395, 486–490, 1998.

Wahner, A., Ravishankara, A. R., Sander, S. P., and Friedl, R. R.: Absorption cross section of BrO between 312 and 385 nm at 298 and 223 K, Chem. Physics Letters, 152, 507–512, 1988.

Wennberg, P. O., Cohen, R. C., Stimpfle, R. M., Koplow, J. P., Anderson, J. G., Salawitch, R. J., Fahey, D. W., Woodbridge, E. L., Keim, E. R., Gao, R. S., Webster, C. R., May, R. D., Toohey, D. W., Avallone, L. M., Proffitt, M. H., Loewenstein, M., Podolske, J. R., Chan, K. R., and Wofsy, S. C.: Removal of stratospheric O_3 by radicals: In situ measurements of OH, HO_2, NO, NO_2, ClO, and BrO, Science, 266, 398–404, 1994.

Wingenter, O. W., Kubo, M. K., Blake, N. J., Smith, Jr., T. W., Blake, D. R., and Rowland, F. S.: Hydrocarbon and halocarbon measurements as photochemical and dynamical indicators of atmospheric hydroxyl, atomic chlorine and vertical mixing obtained during Lagrangian flights, J. Geophys. Res., 101, 4331–4340, 1996.

Zhu, X., Prospero, J. M., Millero, F. J., Savoie, D. L., and Brass, G. W.: The solubility of ferric iron in marine aerosol solutions at ambient relative humidities, Mar. Chem., 38, 91–107, 1992.